NTNU – Trondheim
Norwegian University of
Science and Technology

Wear and corrosion properties of steels used in Tunnel Boring Machines

Christian Kreyberg Grødal

Norwegian University of Science and Technology
Department of Engineering Design and Materials

THE NORWEGIAN UNIVERSITY
OF SCIENCE AND TECHNOLOGY
DEPARTMENT OF ENGINEERING DESIGN
AND MATERIALS

MASTER THESIS SPRING 2012
FOR
Christian Kreyberg Grødal

Wear and corrosion properties of steels used in Tunnel Boring Machines
Slitasje og korrosjon egenskaper for stål benyttet i tunnelboremaskiner

Background
Tunnel Boring Machines (TBM) are used to bore tunnels, a specific area of interest for TBMs is their cutter heads, which is a massive steel structure with hardened steel disc cutters attached.

The disc cutters can encounter all types of geology, from soft clays, slits, sands etc., to soft rock and extremely hard rock, and environments, dry, seawater or even chemicals. These geologies and environments cause the disc cutters to be continuously exposed to wear, wearing them out. Replacing the disc cutters is a considerable part of the total tunnelling costs. A better understanding of the wear and corrosion mechanisms occurring during tunnel boring in different geology and environments can contribute to reducing the disc cutter wear, consequently, reducing the tunnelling costs.

Objective
Steels used in the disc cutters on Tunnel Boring Machines will be investigated. The steels microstructure, hardness, alloying elements and dry wear and tribocorrosion performance will be explored establishing a correlation between the metal properties and the wear environment the metal is exposed to. Rock/soil and water samples will be obtained from field (i.e. active tunnel boring projects) in order to obtain more realistic results.

The following tasks shall be considered in the master thesis work:
- Gathering of samples: selection of steels and field trips to active tunnel boring projects to collect rock, soils and water samples.
- Perform microstructural characterization of all materials used in this work (metallography, SEM, etc).
- Study the dry wear and tribocorrosion performance using lab scale equipment (i.e. rubber wheel, pin-on-disk).

The thesis should include the signed problem text, and be written as a research report with summary both in English and Norwegian, conclusion, literature references, table of contents, etc. During preparation of the text, the candidate should make efforts to create a well arranged and well written report. To ease the evaluation of the thesis, it is important to cross-reference text, tables and figures. For evaluation of the work a thorough discussion of results is appreciated.
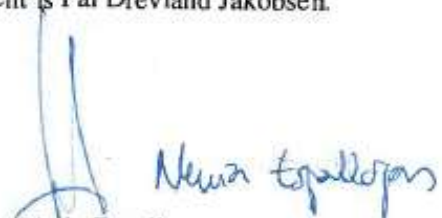
Three weeks after start of the thesis work, an A3 sheet illustrating the work is to be handed in. A template for this presentation is available on the IPM's web site under the menu "Undervisning". This sheet should be updated when the Master's thesis is submitted.

The thesis shall be submitted electronically via DAIM, NTNU's system for Digital Archiving and Submission of Master's thesis.

This master thesis will be performed in cooperation with the department of Civil and Transport Engineering. The co-supervisor at this department is Pål Drevland Jakobsen.

Torgeir Welo
Head of Division

Nuria Espallargas
Assoc. Professor/Supervisor

NTNU
Norges teknisk-
naturvitenskapelige universitet

Institutt for produktutvikling
og materialer

Preface and Acknowledgements

This is a master thesis carried out in cooperation between the Department of Engineering Design and Materials and the department of Civil and Transport Engineering.

This thesis is done to acquire understanding on how the wear on the steel disc cutters used on tunnel boring machines are affected by the microstructure, hardness and alloying elements of the steel. As well as how the different environments the boring is performed in and different additives affects the wear. All laboratory experiments were done at the Tribology Lab and Metallurgy Lab at IPM NTNU.

I would like to thank my supervisors, Nuria Espallargas and Pål Drevland Jakobsen, for giving me this master thesis and for the guidance and support they have given me. I would especially like to thank Pål Drevland Jakobsen for his help to get both practical and theoretical knowledge about TBMs and for his help arranging field trips, and Nuria Espallargas for her help   guidance performing the laboratory experiments.

11/06/2012, Trondheim

Christian Kreyberg Grødal

Summary

In this master thesis experiments were conducted to determine the abrasion-corrosion properties of a steel designed for TBM tunnelling. This was done by three different tests, reciprocal ball-on-plate, rubber wheel and hyperbaric soil abrasion test.

The reciprocal tests were done by rubbing steel balls onto rock obtained from a tunnel boring site in the Faroe Islands. The test were performed in dry conditions, in water from the same site as rock and a mixture of the water and a foam designed for use in hard rock tunnel boring. During these tests no measurable weight loss was produced, but the water and the foam caused some pitting to occur on the steel surface. The water and foam also provided some lubrication, where the foam clearly was the best lubricant by producing elastohydrodynamic lubrication (EHL).

The rubber wheel tests were performed in different combinations of water, sand, oil and a foam specially designed for soft ground tunnel boring. The sands used were sand used for making casting moulds and sand obtained from a soft ground tunnel boring site in Israel. The two different water samples used were obtained from the site in the Faroe Islands mentioned above and the previous mentioned Israel site. The tests showed that adding foam to the sand and water mixture significantly reduced the measured weight loss. However, as for the reciprocal ball-on-plate test, the foam caused pitting to occur. The same corrosion effect was observed for the oil additive, but the oil did not provide enough lubrication to avoid abrasive wear. Consequently, the test with the oil additive produced the biggest weight loss of all the rubber wheel tests.

The hyperbaric soil abrasion tests were performed in the sand obtained at the site in Israel. The sand was tested both dry and saturated with water from Israel. Tests showed that the measured weight loss from these two tests was similar. However, SEM pictures revealed that in the test with sand saturated with water, both abrasion and corrosion had occurred. While in the dry sand, only abrasion had occurred. This indicates that in this test the hardness of the steel and abrasiveness of the sand is more decisive for the weight loss than the corrosivity of the solution.

Sammendrag

I denne master oppgaven har det blitt utført eksperimenter for å bestemme abrasjon-korrosjon egenskapene til et stål designet for bruk i TBM tunnelboring. Dette ble gjort ved å utføre tre forskjellige tester; ball-on-plate, rubber wheel og Hyperbaric Soil Abrasion test.

Ball-on-plate testene ble utført ved å gni en stålkule fram og tilbake på en stein fra et tunnelboreprosjekt på Færøyene. Testene ble utført tørre, i vann fra det samme prosjektet på Færøyene og i en blanding av vannet og et skum beregnet for tunnelboring i hardt berg. Disse testene produserte ikke noe målbart vekttap på stålkulene, men vannet fra Færøyene og skummet forårsaket noe gropkorrosjon på ståloverflaten. Vannet og skummet forårsaket også noe smøring, hvor skummet ga den klart beste smøringen ved å gi elastohydrodynamisk smøring (EHL).

Rubber wheel testene ble utført i forskjellige kombinasjoner av vann, sand olje og et skum spesial designet for tunnelboring i løsmasse. Sandene som ble brukt var støpesand brukt til å lage støpeformer og en sand som hadde blitt hentet fra et løsmasse tunnelboreprosjekt i Israel. De to forskjellige vannprøvene brukt var vann fra prosjektet på Færøyene og vann fra prosjektet i Israel. Testene viste at vekttapet ble vesentlig redusert når skummet ble tilsatt sand og vann blandingen. Men, i likhet med ball-on-plate testen, forårsaket skummet en del gropkorrosjon. Tilsats av olje hadde også den samme korrosive effekten, men oljen klarte ikke å produsere nok smøring til å separere ståloverflaten fra sandpartiklene. Noe som førte til at blandingen med tilsatt olje hadde det største vekttapet av alle rubber wheel testene utført.

Hyperbaric soil abrasion testen ble utført i sanden hentet fra prosjektet i Israel. Testen ble utført med både tørr sand og mettet med vann fra det samme prosjektet. Testene viste at det målte vekttapet fra disse to testene var i samme størrelsesorden. SEM bildene viste imidlertid at testen med sand mettet med vann hadde resultert i både abrasjon og korrosjon, mens testen med tørr sand kun gav abrasjon. Dette indikerer at stålets hardhet og abrasiviteten til sanden er mer avgjørende for vekttapet enn korrosiviteten til løsningen.

Table of Contents

1 Abbreviations

TBM	-	Tunnel Boring Machine
EPBM	-	Earth Pressure Balanced Machine
VHN	-	Vickers Hardness Number
AMC	-	Abrasive Mineral Content
AV/AVS	-	Abrasion Value
SAT	-	Soil Abrasion Test
R_a	-	Roughness Average
R_q	-	Root Mean Square Roughness
EHL	-	Elastohydrodynamic Lubrication
BCC	-	Body-Centred Cubic
FCC	-	Face-Centred Cubic
HCP	-	Hexagonal Close-Packed
RA	-	Retained Austenite
SEM	-	Scanning Electron Microscope
XRF	-	X-ray Fluorescence
COF	-	Coefficient of Friction
EDS	-	Energy Dispersive Spectrometry
E_{corr}	-	Corrosion Potential
rpm	-	Revolutions per Minute

2 Introduction

Tunnel Boring Machines (TBM) are used to bore tunnels, and can encounter all types of geology and mineralogy/chemistry, from soft clays, slits, sands etc., to soft rock and extremely hard rock.

In tunnelling, the combined action of abrasion of the cutters rolling against the rock and the mineralogy/chemistry of the rocks might generate an abrasion-corrosion scenario. This process is the so-called tribocorrosion in the tribology literature and employs the mechanical and chemical effects in one degradation mechanism. Tribocorrosion is a material deterioration or transformation caused by wear and corrosion simultaneously. To determine tribocorrosion, it is not possible to look at the corrosion and wear separately, because the wear is influenced by corrosion and corrosion is influenced by wear. This combined effect is called Synergy, which enhances the material removal rates and can be a source of additional defects that might influence the mechanical properties of the TBM structure.

A specific area of interest for this master thesis is the TBMs cutter head, which is a massive steel structure with hardened steel disc cutters. The disc cutters are continuously wearing out in many different environments depending on the mineralogy of the rocks and/or soils, leading to a substantial part of the tunnelling cost. In addition the effect of foam additives on wear is also an area of interest in this master thesis.

There are two main types of foam which will be studied in this master thesis. One designed for boring in hard rock and the other one for boring in soil. The purpose with the foam used in hard rock boring is to reduce the friction, cool the cutter tools and to reduce the amount of dust in the air. The purpose of the foam used in soil boring is to reduce the wear on the cutter tools.

In this master thesis the abrasion-corrosion properties of a cutter steel machined into small test specimens have been tested. These specimens will be exposed to different wear test in different environments. The tests performed in this master thesis are:

- Reciprocal ball-on-plate
- Rubber Wheel
- Hyperbaric Soil Abrasion Test

In this master thesis two different foam additives were tested MEYCO ABR 5 and MEYCO SLF41 designed for use in hard rock and soil, respectively.

In order to be able to replicate the conditions during tunnel boring, the samples used in this master thesis were collected at on-going tunnel boring sites in The Faroe Islands and Israel and the cutter steel used was from an unused cutter ring from Robbins.

The project in the Faroe Islands was a hard rock tunnel boring site. The purpose of this tunnel was to collect water from small rivers for use in hydropower plants. Consequently, the cutter tools would be exposed to water during the boring operation. The project in Israel on the other hand was a soft ground tunnel boring project. The boring was performed beneath the sea bed. Consequently, in this project the cutter tools were exposed to water coming from the sea above, causing a corrosive environment.

The experimental setups in this master thesis were used for simulating the abrasion-corrosion conditions of the tunnel boring environment. The reciprocal ball-on-plate setup causes a wear scenario on the rocks which is compatible with the scenario during tunnel boring in rock. However, the Rubber Wheel setup is not completely compatible with the wear scenario during soft grounds (soils). Consequently, the wear from the soil tests are not entirely consistent with the wear occurring during soft ground tunnel boring either. The Hyperbaric Soil Abrasion Test setup is designed to give a better replication of the conditions present during boring in soft ground. However, this test is a new test and therefore little comparable test results exist.

3 Theory

3.1 Tunnel Boring Machines (TBM)

Excavation by a TBM is done by a circular cross section. TBMs minimize the disturbance of the rock and make it possible to follow the plan tunnel profile precisely [1]. It is important to know as much as possible about the different geological and geo-mechanical characteristics of the soil/rock to be excavated [2]. There are different types of TBMs applicable to different types of geology. A more detailed description will be given in the following two chapters; Hard Rock TBMs and Soft Ground TBMs.

It is important to get an indication on the characteristics of the rock/soil to be encountered before the boring process. The characterisation of rocks and soils will be described in the chapters below. It is also important to know something about the hydro-geological conditions such as the rock/soil density, cohesion, permeability, expected water pressure, seasonal/tidal variations, pH-value, etc [2]. Especially for tunnel boring in soil it is important to be able to determine the soil/water pressure so that it is possible to determine the pressure needed to keep the tunnel face stable during boring.

3.1.1 Hard Rock TBMs

There are two main types of TBMs used in hard rock: the open gripper-type and the shielded type machines. The open gripper-type was used in the tunnel boring project visited on the Faroe Islands. The cutter head excavation process for the two types is the same. The cutter heads have a certain number of disc cutters to excavate the hard rock, see Figure 1 and Figure 2. The excavation process is performed by the cutter head being pressed against the excavation face, causing the cutters to penetrate into the rock. This leads to severe tensile and shear stresses, which again causes pulverisation and chips due to crack formation. Due to difference in hardness of the rocks at the tunnel face and the roughness caused by the chipping of the rock, the disc cutter will experience a hammering effect with high peak loads. The failure mechanism, causing chipping, under the cutter is shown in Figure 3 [2]. In addition to the normal wear experienced on the cutter discs during boring this hammering effect may cause fatigue to occur.
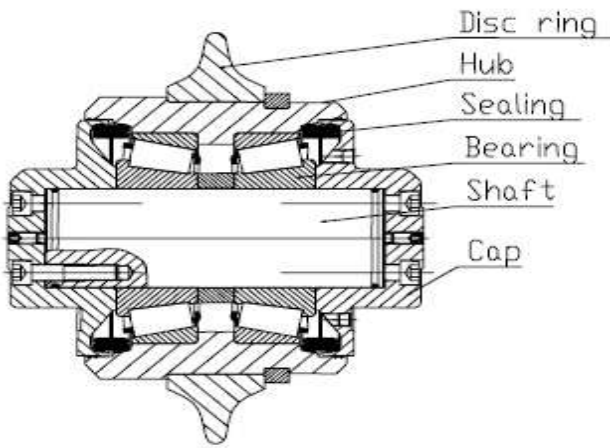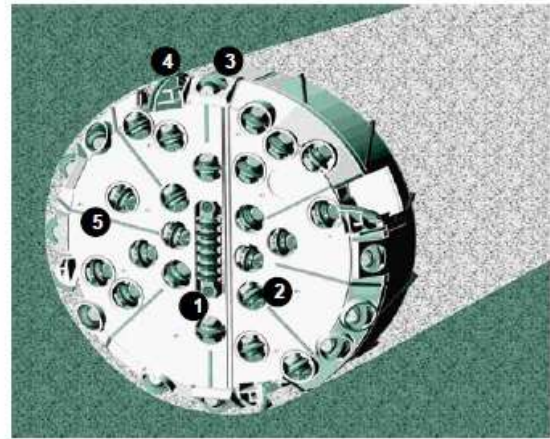
Figure 1 Typical disc cutter design [2].

1 Centre Cutter
2 Face Cutter
3 Gauge Cutter
4 Scraper
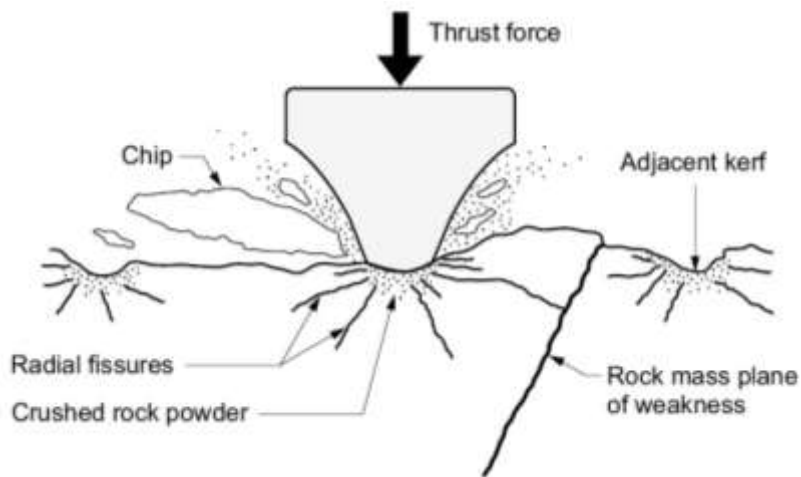5 Wear Plates

Figure 2 Cutter Head front view [2].

Figure 3 Failure mechanism under the cutter edge [3].

Characterisation of Rocks

The characteristics of the rocks encountered during tunnel boring determine the performance of the TBM, including excavation rates and cutter consumption. Strength, toughness, hardness and abrasivity are important parameters influencing the characteristic of a rock. These parameters are described below. Another important parameter is the weakness planes, which will have a strong influence on the boring process. The weakness planes will also influence the tests determining the other parameters. For example, when determining the strength of a rock, the weaknesses along bedding- and foliation planes and the distribution of cracks and flaws will not be the same in every test specimen. Consequently, the results of the various tests will vary from specimen to specimen as well [4].

The intact rock surface, fragments of rock and crushed rock powder are causing abrasive wear on the cutters. The toughness, strength and hardness are all influencing the amount of rock and powder produced. While the hardness and the strength are parameters affecting the rock´s abrasivity the most. For a rough indication of the abrasiveness of the abrasivity of a rock the Moh's hardness may be used. To obtain a more accurate value it is possible to use the Cerchar test or Abrasion Value test (AV/AVS). Figure 4 shows the Abrasion Value test rig [4].
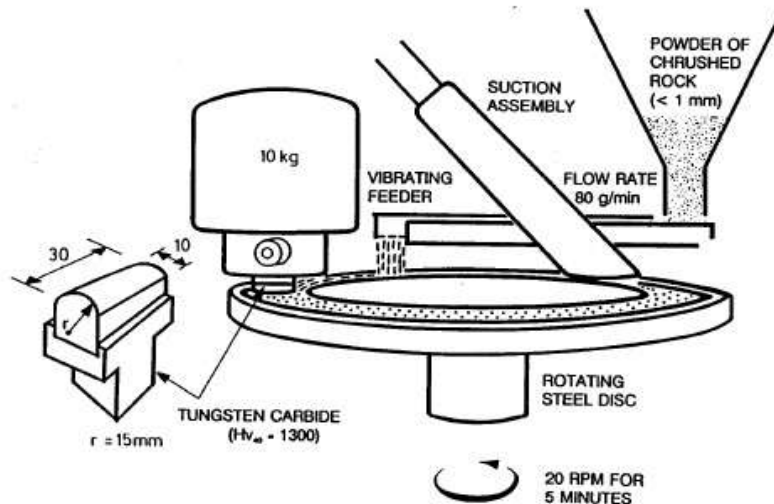
Figure 4 The Abrasion Value test [4].

3.1.2 Soft Ground TBMs

The boring process in soft ground is similar to that in hard rock, with regards to thrusting and rotation. Soft ground is often encountered when infrastructure tunnels are made under urban areas. It is important to be able to execute the tunnel boring in a safe, efficient and economical way, despite unforeseen alteration in the ground conditions. Usually, the simplest way is to treat the ground in such a way that the conditions become manageable for the TBM. This can be done by injecting a foam additive at the font of the TBM. However, depending on the geology of the soil, soft ground TBMs may also be equipped with disc cutters similar to those for hard rock [2]. When these disc cutters encounter areas of rocks, they are experiencing peak loads giving a hammering effect.

Characterisation of Soils

The reason why it is important to characterise the soil are for the same reasons described for characterisation of rocks. There are few test methods to describe the characteristics of soils. Typical tests are Vickers Hardness Number (VHN), Moh's hardness, quartz content and abrasive mineral content (AMC) [5]. In addition there are some soil abrasivity tests like the Nordic Ball Mill test [6]. However, the former two tests measure the abrasion of soils induced by the steel and not the other way round. Lately a new abrasion test for soils has been tried out. This is the new NTNU Soil Abrasion Test (SAT) and is based on the already existing AVS test, see Figure 4 [5]. The only difference between the AVS and SAT test is that the AVS uses crushed rock powder (<1 mm) and the SAT uses sieved soil (<4 mm) [5].

3.2 Tribology

3.2.1 Surface roughness

The surfaces on components used in TBMs are far from ideally smooth, and exhibit some roughness. These characteristic surface features may influence friction, wear and lubrication independent of the underlying material [7].

Surface roughness characterisation

A common way to describe the surface roughness is by among others the "roughness average" (R_a) or "root mean square roughness" (R_q), where the roughness average parameter is the most commonly used in engineering practice[7].

The R_a gives the average roughness over the entire length measured on the sample. Consequently, a non-typical peak or valley will have little influence on the final roughness value. This can be problem can be resolved by using the R_q parameter. The R_q parameter is more sensitive to deviations than R_a because it is weighted by the square of the heights [7]. These two parameters are defined in Equation 1 and Equation 2 below. Where L is the sampling length and z is the height of the profile along x.

Equation 1 [7].

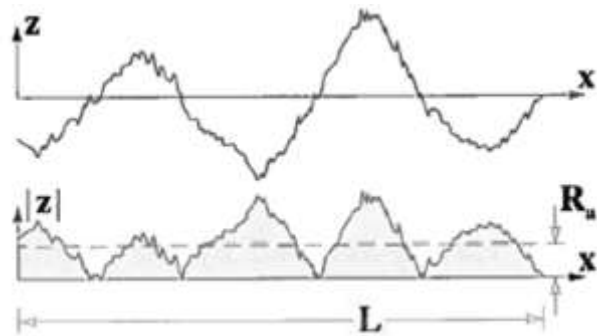Roughness average, R_a

$$R_a = \frac{1}{L}\int_0^L |z|\,dx$$

Figure 5 Roughness average, R_a [7].

Equation 2 [7].

Root mean square roughness, R_q

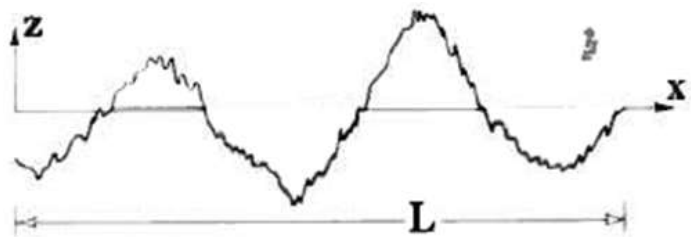$$R_q = \sqrt{\frac{1}{L}\int_0^L z^2\,dx}$$

Figure 6 Root mean square roughness, R_q [7].

3.2.2 Lubrication

During excavation with TBMs the forces acting on the tunnel face and the cutter discs are very high, leading to a significant amount of wear on the cutter discs. In order to prevent this, some of the TBMs are equipped with some sort of lubricating system, spraying a lubricant on to the tunnel face. Due to the high pressures acting in the contact area between the rock and the disc cutter, the lubricating regime present is elastohydrodynamic lubrication (EHL). The lubrication not only helps to reduce the wear occurring on the cutter discs, but also reduces the amount of dust in the air and cools the steel discs during hard rock tunnel boring.

EHL

Elastohydrodynamic lubrication is a form of hydrodynamic lubrication where the elastic deformation of the contacting bodies and the changes of viscosity with pressure are basic principles. The lubricating films in EHL are very thin; from 0.1 to 1 µm, but are enough to separate the interacting surfaces. Thus avoiding wear due to friction. There are three effects that play a vital role in the formation of the lubricating films in EHL [7]:

- The hydrodynamic film formation.
- The modification of the film geometry by elastic deformation.
- The transformation of the lubricant`s viscosity and rheology under pressure.

Hydrodynamic Film Formation

In order for hydrodynamic lubrication to occur there are two conditions that need to be fulfilled:

- Two surfaces must move relative to each other with sufficient velocity for a load carrying lubricating film to be generated.
- Surfaces must be inclined or tilted at some angle to each other.

However, there are two exceptions to this last rule; hydrodynamic pressure can be generated between parallel stepped surfaces or surfaces moving against each other. Figure 7 shows the principles of hydrodynamic pressure generation [7].
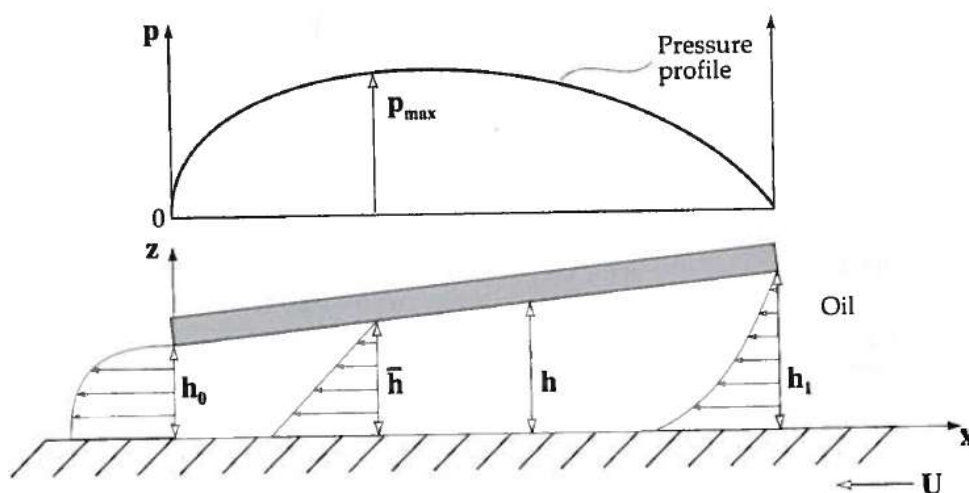

Figure 7 Principle of hydrodynamic pressure generation between non-parallel surfaces [7].

All hydrodynamic lubrication can be expressed in the form of an equation derived from Reynolds equation [7]. However, in most engineering applications the processes present are too complicated to be described easily by exact mathematical equations. Therefore, several simplifications have to be made[7]:

- Body forces are neglected.
- Pressure is constant through the film.
- No slip at the boundaries.
- Lubricant behaves as a Newtonian fluid.
- Flow is laminar.
- Fluid inertia is neglected.
- Fluid density is constant.
- Viscosity is constant throughout the generated fluid film.

Equation 3 shows the Reynolds equation derived by consideration of continuity of flow in a column (Figure 8).

$$\frac{\partial}{\partial x}\left(\frac{h^3}{\eta}\frac{\partial p}{\partial x}\right) + \frac{\partial}{\partial y}\left(\frac{h^3}{\eta}\frac{\partial p}{\partial y}\right) = 6\left(U\frac{dh}{dx} + V\frac{dh}{dy}\right) + 12(w_h - w_0) \qquad \text{Equation 3 [7].}$$
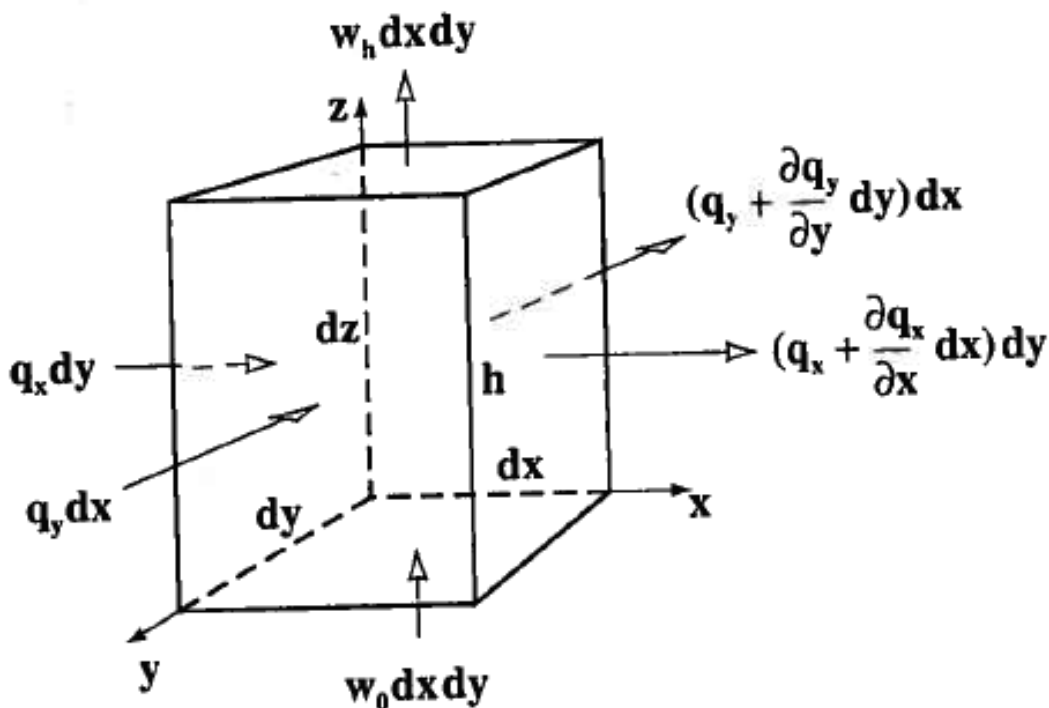
Figure 8 Continuity of flow in column [7].

Modification of Film Geometry by Elastic Deformation

Regardless of a materials modulus of elasticity, a surface in Hertzian contact deforms elastically. The effect of elastic deformation on the lubricant film is mainly to introduce a central region of quasi-parallel surfaces between inlet and outlet wedges. This is shown in Figure 9, where two bodies in elastic contact are illustrated [7].
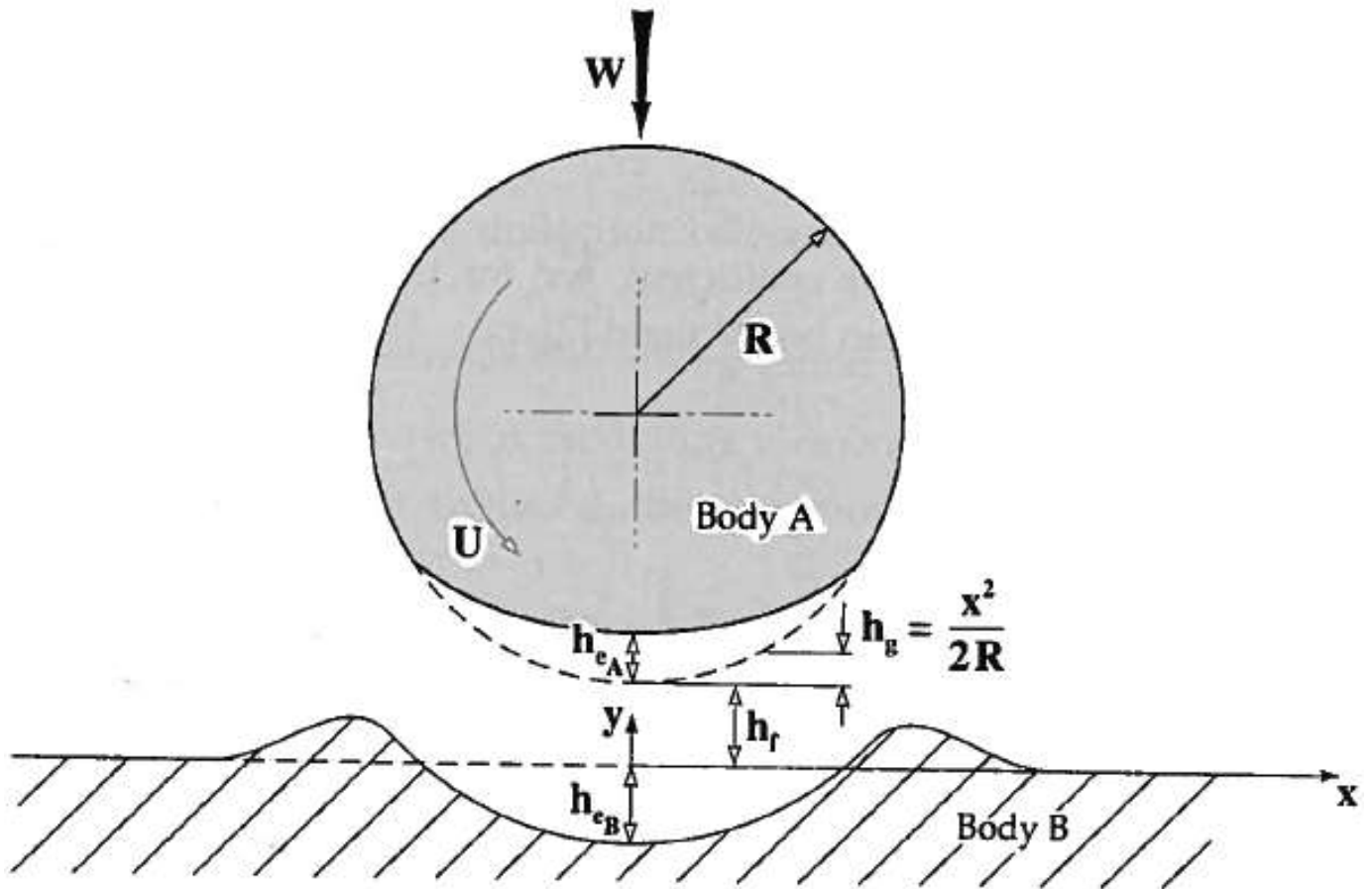
Figure 9 Effects of local elastic deformation on the lubricant film profile [7].

Where:

h_f is the film thickness, which is constant [m];

h_e is the combined elastic deformation of the solids [m], i.e., $h_e = h_{eA} + h_{eB}$;

h_g is the separation due to the geometry of the undeformed solids [m];

R   is the radius of the ball [m].

Transformation of Lubricating Viscosity and Rheology under Pressure

The difference in geometry of the contacting surfaces induces an intense concentration of load over a very small area for almost all Hertzian contacts of practical use. The liquid separating the two surfaces are exposed to extreme pressures many times higher than in hydrodynamic lubrication, pressures from 1 to 4 GPa have been found. For many mineral oils, and some other fluids used in tribological situations, the viscosity increases significantly with pressure. This is a phenomenon known as piezoviscosity, and can be modelled by the Barus equation shown below [7, 8].

$$\eta_p = \eta_0 e^{\alpha p} \qquad \text{Equation 4 [7].}$$

Where:

η_p is the lubricant viscosity at pressure "p" and temperature "θ" [Pa·s];

η_0 is the viscosity at atmospheric pressure and temperature "θ" [Pa·s];

α   is the pressure-viscosity coefficient [m^2/N].

3.2.3 Wear mechanisms

The most common wear mechanism for TBMs is abrasive wear. Abrasive wear occurs on the surface of a component due to relative motion to an adjacent surface with harder asperities or hard particles trapped at the interface [8]. The two modes of abrasive wear are referred to as Two-body and Three-body abrasive wear, as shown in Figure 10 and Figure 11, respectively [7]. The two-body abrasive wear occurs when the harder asperities or firmly held grits act like a cutting tool (Figure 10). Three-body abrasive wear occurs when particles are free to roll and slide over the surfaces of both components (Figure 11). The three-body abrasive wear is ten times lower than two-body wear, this is because three-body wear have to compete with other wear mechanisms. Both these two modes of abrasive wear can occur during tunnel boring. Three-body wear can occur due to chipped hard rock particles present between the rock and steel surfaces. Any particles stuck due to the surface roughness on the rock, are removed by the steel surface. In addition, an increase in the temperature can cause two-body wear to occur. The effect of temperature can be divided into two groups: influenced by the temperature of the surroundings and induced by plastic deformation. For this project the latter case is most relevant, because the temperature of the surroundings is not high enough to affect the steel properties. While there are sufficient plastic deformations present to obtain the temperature needed to soften the steel. The plastic deformations causing increased temperature are often induced by high speeds [7]. However, evidence of localised melting have been found in wear tests at sliding speeds as low as 1 ms^{-1} [8]. When the temperature increases because of plastic deformation due to three-body wear, the contact period would be relatively short. This causes only the deformed material to soften, leaving the grits hardness unaltered [7]. Consequently, rock particles that are stuck will not be removed, but rather cause two-body wear increasing the wear on the steel surface.
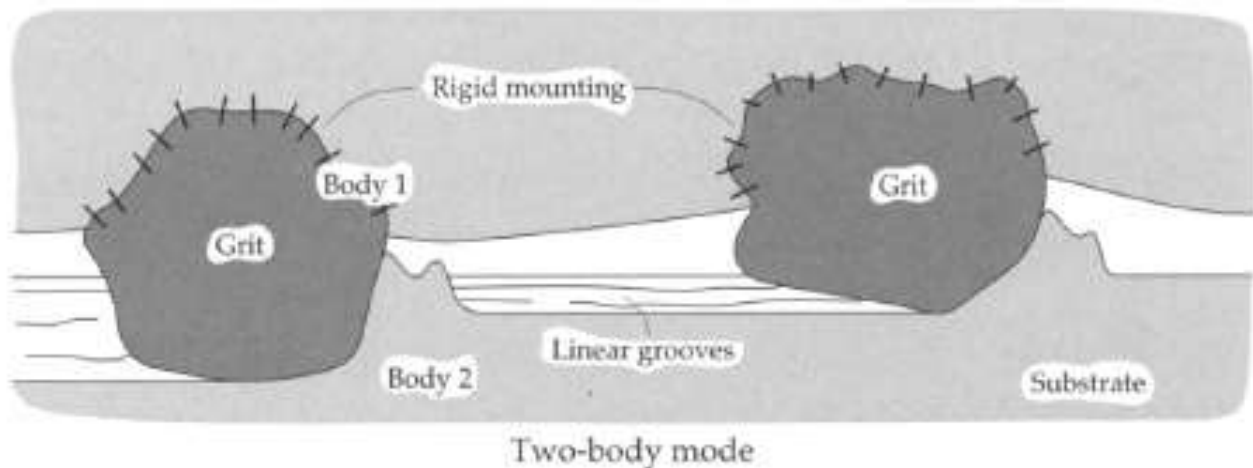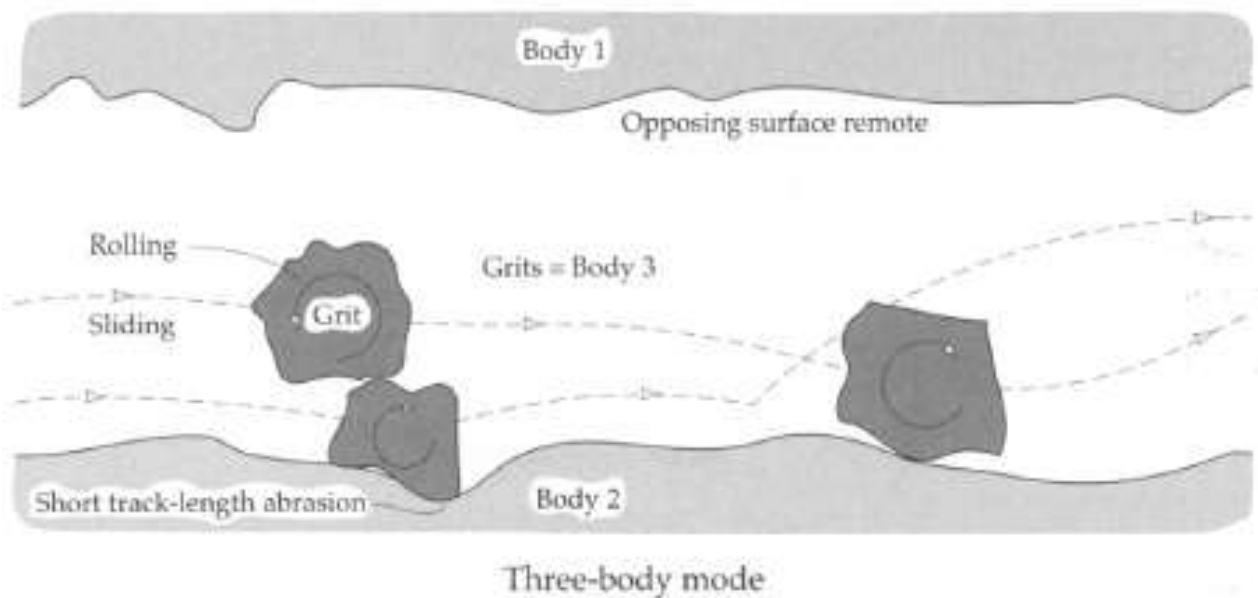

Figure 10 Two-body wear [7].

Figure 11 Three-body wear [7]

Because of the different types of wear situations, different types of abrasive wear can occur [9]. The next section will look at cutting, fracture and fatigue due to abrasive wear. This is because these are considered to occur during tunnel boring due to the combination of hard particles, high forces and numbers of wear cycles the disc cutters are exposed to. It is important to remember that normally there is not one single mechanism responsible for the wear, but a combination of several.

Cutting/Ploughing

When the harder surfaces asperities are pressed into the softer material in combination with tangential motion, the result is cutting/ploughing removing the softer material [9]. The material underneath the surface exposed to abrasion is plastically deformed. This subsurface deformation causes the occurrence of strain hardening, which may reduce the abrasive wear. This is shown in Figure 12 [7].
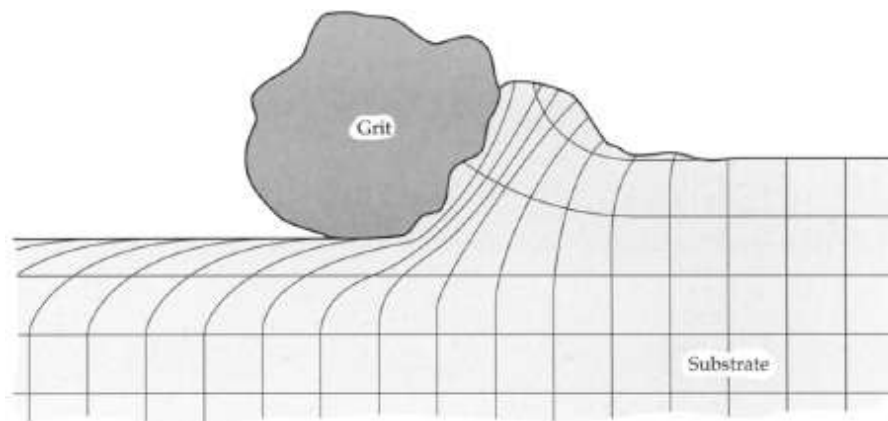
Figure 12 Ssubsurface deformation by ploughing [7].

Fracture

This mechanism is caused by the surface traction exerted by the harder asperities, causing plastic shear deformation of the softer material. As the loading is repeated, deformation is building up. Eventually cracks are formed in the vicinity of already existing voids or inclusions. Once a crack is formed, additional loading cause it to propagate. Consequently, the cracks reach the surface, causing chips to break off [8]. This is shown in Figure 13.
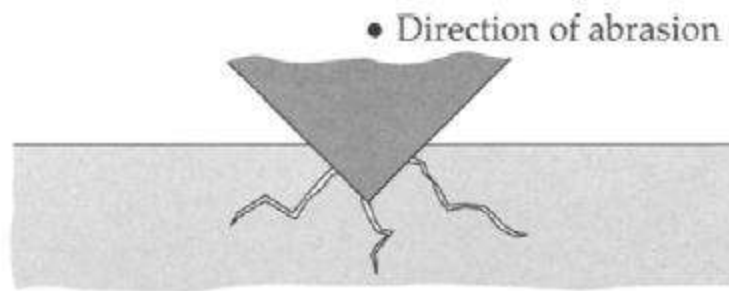

Figure 13 Fracture due to abrasive deformation [7].

Fatigue

The mechanism of fatigue is similar to that of fracture. Fatigue is caused by repeated strain causing grits or asperities to deform the surface. This will cause cracks to nucleate from material defects. However, unlike fracture, fatigue may eventually occur after being operational for many hours and at a much lower load. Particles from fatigue wear are characteristically much larger than those from plain abrasive wear, and once a particle chip off from one of the surfaces, further deterioration usually follows rapidly [8]. This is shown in Figure 14.

1) Crack initiation as a result of fatigue processes   2) Primary crack propagation along slip plane

3) Secondary crack initiation   4) Secondary crack propagation and formation of wear particle
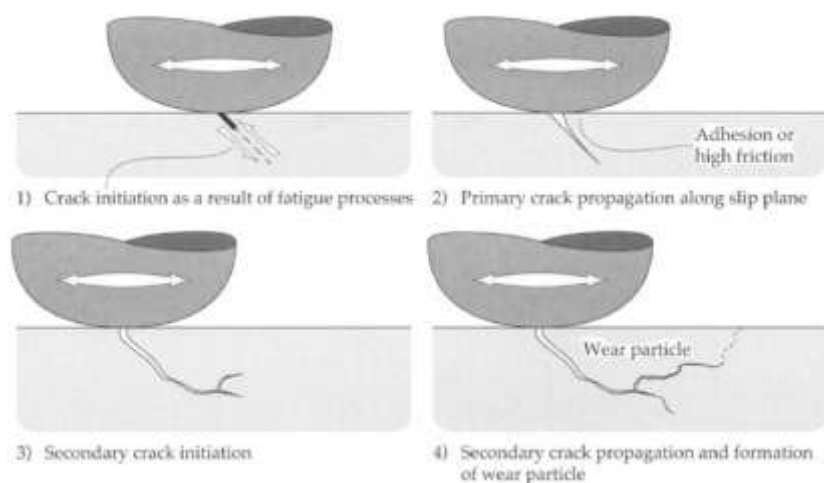
Figure 14 Fatigue wear [7].

3.2.4 Analytical models of abrasive wear

During two-body abrasive wear a large proportion of the abraded material is thought to be displaced to the sides of the grit path, instead of just disappearing. For a ductile material the displaced portion is observed as a pair of walls to the edges of the abrasion groove (Figure 15) [7].
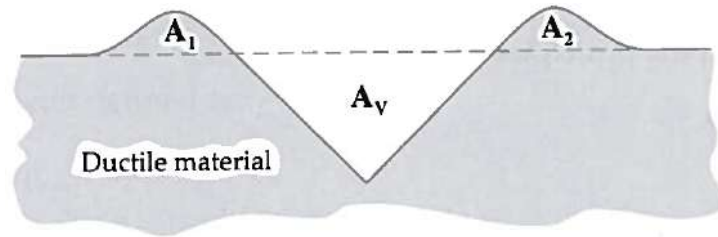

Figure 15 Model of material removal and displacement in ductile abrasive wear [7].

The parameter "f_{ab}" (Equation 5) gives the ratio of the amount of material removed from the surface by a grit to the volume of the wear groove. For a ductile material this parameter can be calculated from Equation 5 below [7].

$$f_{ab} = 1 - (A_1 + A_2)/A_V \qquad \text{Equation 5 [7].}$$

Where:

A_V is the cross-sectional area of the wear groove [m^2];

$(A_1 + A_2)$ is the cross-sectional area of the material displaced at the edges of the groove (Figure 15) [m^2].

For abrasive wear of brittle materials there is no displaced material at the edges of groove, but rather a widening of the groove due to chipping at the side of the grooves as shown in Figure 16.
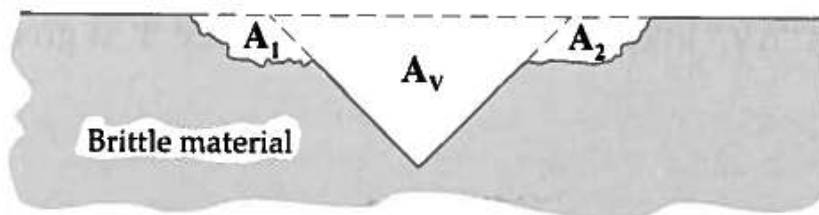
Figure 16 Model of material removal in brittle abrasive wear [7].

This causes the areas A_1 and A_2 to become negative. Consequently, the expression for f_{ab} is modified to:

$$f_{ab} = 1 - |A_1 + A_2|/A_V \qquad \text{Equation 6 [7].}$$

The volumetric wear loss "ΔV_l" [m^2] in terms of the sliding distance "L" is given by Equation 7 below:

$$\Delta V_l = \frac{\Delta V}{L} = f_{ab} A_V \qquad \text{Equation 7 [7].}$$

3.2.5 Particle shape

The amount of wear occurring is also dependent on the size and shape of the abrasive particles. However, there are hundreds of ways to describe shapes numerically by dimensionless expressions and there are only a few relatively common combinations [10]. For example; the size of a particle can be defined by the minimum size of a sphere enclosing the entire particle. While the particles geometry often is defined as how the particle differs from an ideal sphere [7]. Table 1 summarizes some of the most commonly used combinations.

Table 1 Different commonly used shape descriptors [10].

Shape descriptor	Formula	
Form factor	$FF = \dfrac{4\pi \cdot Area}{Perimeter^2}$	Equation 8.
Roundness	$R = \dfrac{4 \cdot Area}{\pi \cdot Maximum\ Diameter^2}$	Equation 9.
Aspect Ratio	$AR = \dfrac{Maximum\ Diameter}{Minimum\ Diameter}$	Equation 10.
Compactness	$C_P = \dfrac{\sqrt{\left(\frac{4}{\pi}\right) \cdot Area}}{Maximum\ Diameter}$	Equation 11.
Circularity	$C_C = \sqrt{FF} = \dfrac{\sqrt{4\pi \cdot Area}}{Perimeter}$	Equation 12.
Effective diameter	$ED = 2\sqrt{\dfrac{Area}{\pi}}$	Equation 13.

All of these shape descriptors captures some aspects of shape, however, visually different shapes can give similar values for any of these descriptors. Figure 17 shows four variations of one basic shape and shows the Form factor and Aspect Ratio (AR) belonging to each shape.
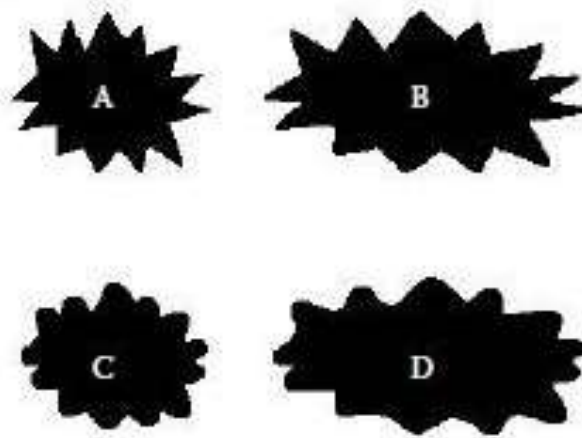

Figure 17 Shape variations [10].

Table 2 Variations of shape descriptors for similar shapes [10].

Shape	Form factor	Aspect Ratio
A	0.257	1.339
B	0.256	2.005
C	0.459	1.294
D	0.457	2.017

3.3 Corrosion mechanisms

Because the steel to be investigated in this project is an active metal in water at neutral and acid pHs, the corrosion mechanism to be prevailing is uniform corrosion and eventually pitting. Uniform corrosion causes the whole surface to corrode with an approximately equal rate, see Figure 18. Uniform corrosion is normally not considered as a dangerous corrosion type because it is easy to predict the thickness reduction rate and available protection methods manage to reduce the corrosion rate to an acceptable level [11]. However, the use of corrosion protection methods is not common in the tunnel boring industry. Therefore uniform corrosion can contribute to the total wear rate of the disc cutters.
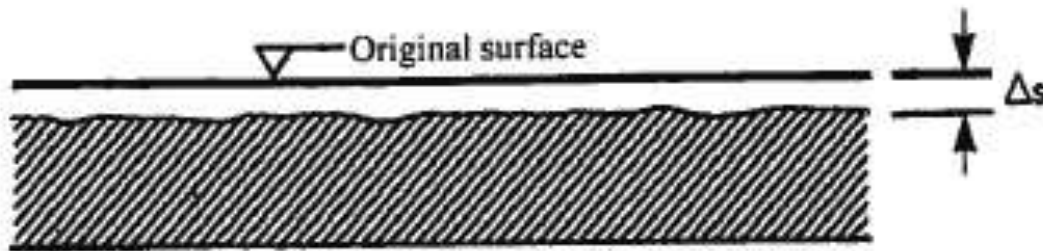
Figure 18 Uniform corrosion, where Δs is the amount of corrosion occurred measured in millimetres from the original surface. [11].

In order for corrosion to occur the metal has to be exposed to an electrolytically conducting liquid (an electrolyte) and the electrical circuit has to be closed by ion conduction through the electrolyte. The corrosion process consists of an anodic and a cathodic reaction [11]. In the anodic areas the following reaction takes place:

$$Fe \rightarrow Fe^{2+} + 2e^-$$ Equation 14 [12].

When iron corrodes, the rate is usually controlled by the cathodic reaction, which, in general, is much slower [12]. In deaerated water, the cathodic reaction is:

$$H^+ \rightarrow {}^1\!/_2\, H_2 + 1e^-$$ Equation 15 [12].

However, the cathodic reaction can be accelerated by dissolving oxygen in a process called depolarization, in accordance with the following reaction:

$$2H^+ + \tfrac{1}{2}O_2 \rightarrow H_2O + 2e^- \qquad \text{Equation 16 [12].}$$

$$H_2O \rightarrow H^+ + OH^- \qquad \text{Equation 17 [12].}$$
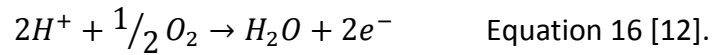
By combining Equation 16 and Equation 17 we obtain Equation 18:

$$\tfrac{1}{2}O_2 + H_2O \rightarrow 2OH^- + 2e^- \qquad \text{Equation 18 [12].}$$
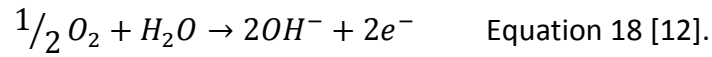
Finally, combining Equation 14 and Equation 18 we obtain the reaction for the overall corrosion process:

$$Fe + H_2O + \tfrac{1}{2}O_2 \rightarrow Fe(OH)_2 \qquad \text{Equation 19 [12].}$$
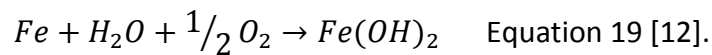
$Fe(OH)_2$ forms a layer/barrier that oxygen has to diffuse through in order to continue the corrosion process further. However, $Fe(OH)_2$ is not stable and with access to oxygen and water it oxidizes to an iron hydroxide, $Fe(OH)_3$, which is the typical red/brow rust [11, 12]. The iron hydroxide film is causing a lowering of the corrosion rate because the diffusion rate of oxygen is also lowered as the film gets thicker [12]. Figure 19 shows the corrosion process present, for a hypothetical divalent metal M.
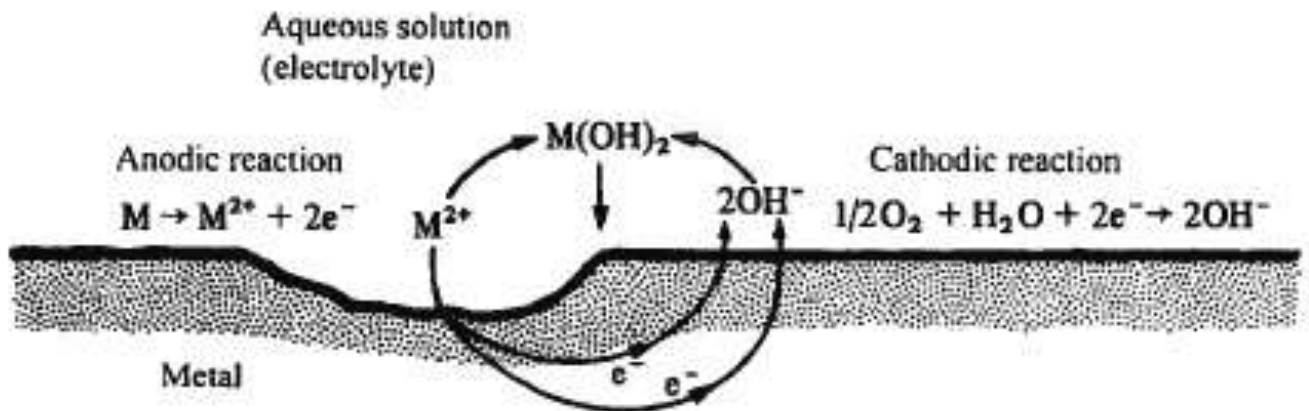
Figure 19 Corrosion of a divalent metal M in an electrolyte containing oxygen [11].

3.3.1 Effect of Dissolved NaCl

The tests conducted in this master thesis are performed in liquids obtained from real tunnel boring projects. At one of the projects the excavation was performed underneath the sea bed, causing the liquid to contain high concentrations of NaCl. The effect of NaCl concentration on corrosion if iron in air-saturated water at room temperature is shown in Figure 20. The corrosion rate first increases with salt content and then decreases, reaching a corrosion rate at NaCl-saturation (26 % NaCl) that is lower than for distilled water. The corrosion rate is controlled by the oxygen depolarisation (Equation 16) throughout the NaCl concentration range. The reason why the corrosion rate reaches a maximum at about 3 wt. % NaCl and then decreasing are because of this. An increase in the concentration of NaCl results in a decrease of the solubility of oxygen, explaining the lower corrosion rates at the higher NaCl concentrations. The initial rise in corrosion rate can be related to a change in the protective nature the diffusion-barrier rust film that forms on corroding iron. Because of the distilled water´s low conductivity, anodes and cathodes must be located relatively near to each other. This causes the formation of OH^- ions at the cathode sites in accordance to Equation 18. They are always in the proximity of Fe^{2+} ions forming at nearby anodes, resulting in a film of $Fe(OH)_2$ adjacent to and adherent to the metal surface. This film provides an effective diffusion-barrier film. However, NaCl solutions have a greater conductivity, thus, additional anodes and cathodes can operate much further apart from each other. At such cathodes, OH^- does not react immediately with $FeCl_2$ formed at the anodes. Instead, they diffuse into the solution, reacting to form $Fe(OH)_2$ away from the surface. Because of this a protective barrier layer does not form at the metal surface. Consequently, more dissolved oxygen can reach the cathodic areas. Above 3 wt. % NaCl the decrease in dissolved oxygen becomes more important than the change in diffusion-barrier layer. Consequently, the corrosion rate decreases [12].
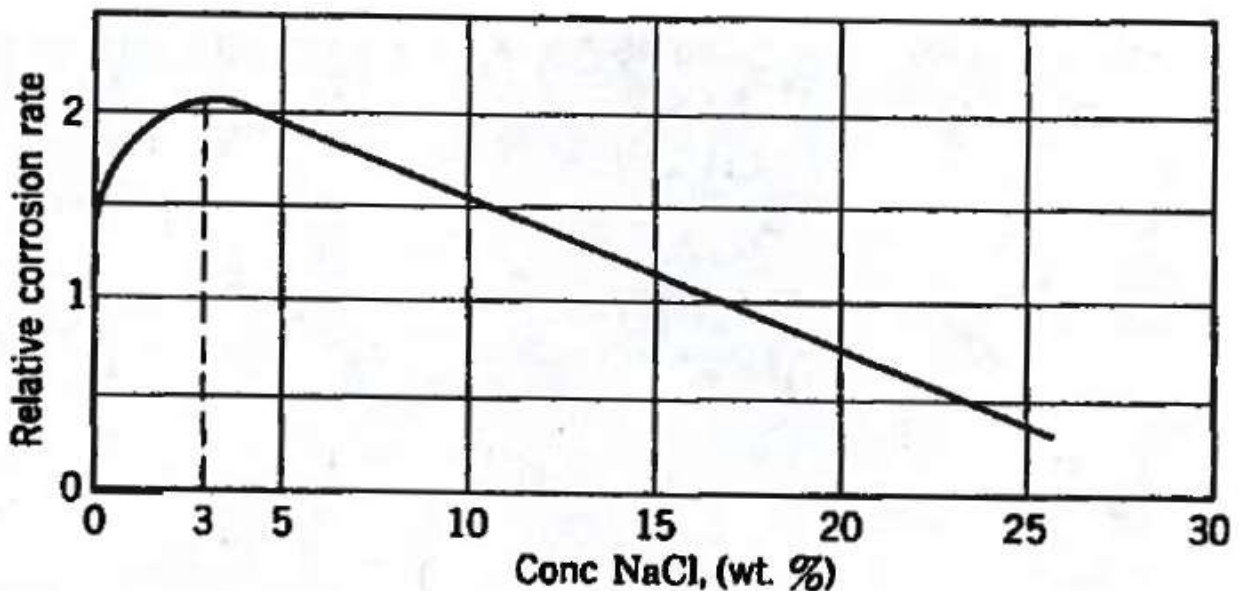

Figure 20 Effect of NaCl concentration on corrosion of iron in aerated solutions, room temperature [12].

3.3.2 Pourbaix diagram

In fluids pH is an important parameter that affects the equilibrium potential for several of the equilibrium reactions occurring. Based on this, Marcel Pourbaix created a pH-potential diagram, also known as a Pourbaix diagram. The Pourbaix diagram is a graphical representation of Nernst´s equation for the relevant reactions. The Pourbaix diagram for iron in water and 3.5 wt. % NaCl at 25 °C is shown in Figure 21 and Figure 22, respectively [11]. The letters a-f represents the following reactions:

a) $Fe^{2+} + 2e = Fe$ Equation 20 [11].
b) $Fe_3O_4 + 8H^+ + 8e^- = 3Fe + 4H_2O$ Equation 21 [11].
c) $Fe_3O_4 + 8H^+ + 2e^- = 3Fe^{3+} + 4H_2O$ Equation 22 [11].
d) $Fe_3O_4 + 6H^+ + 2e^- = 2Fe^{2+} + 3H_2O$ Equation 23 [11].
e) $O_2 + 4H^+ + 4e^- = 2H_2O$ Equation 24 [11].
f) $2H^+ + 2e^- = H_2$ Equation 25 [11].
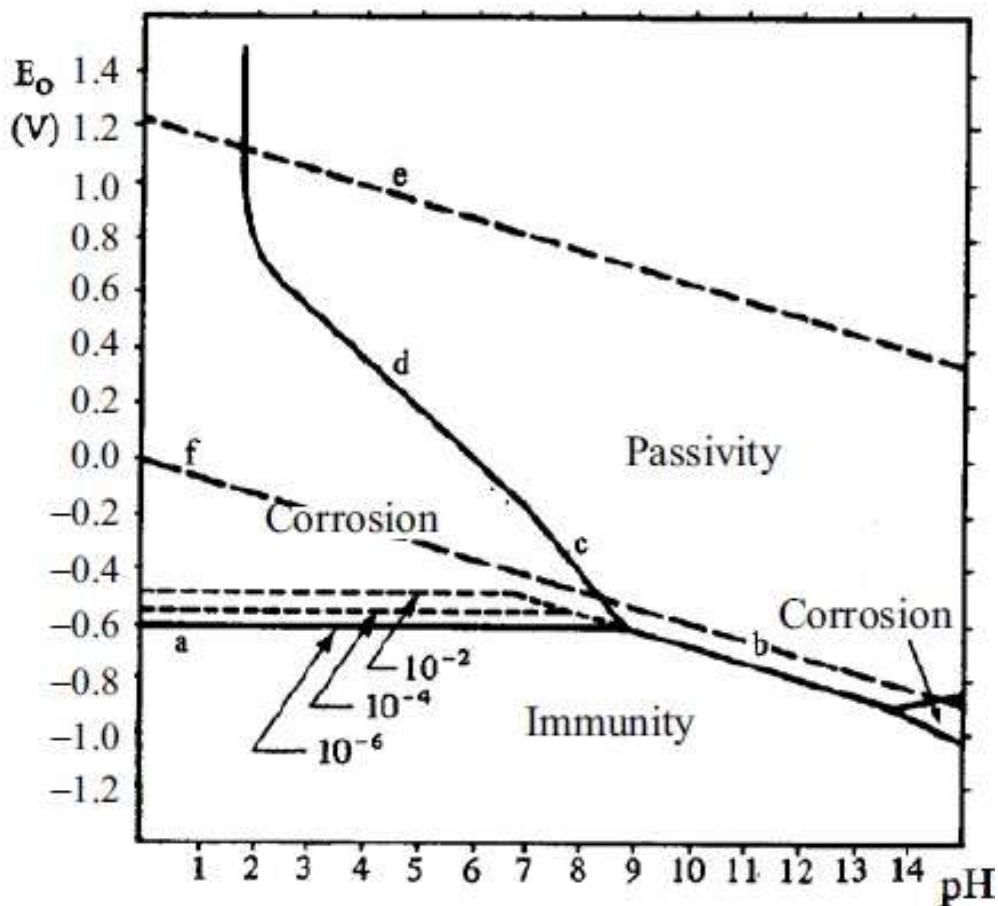
Figure 21 Pourbaix diagram for iron in water at 25° C [11] .
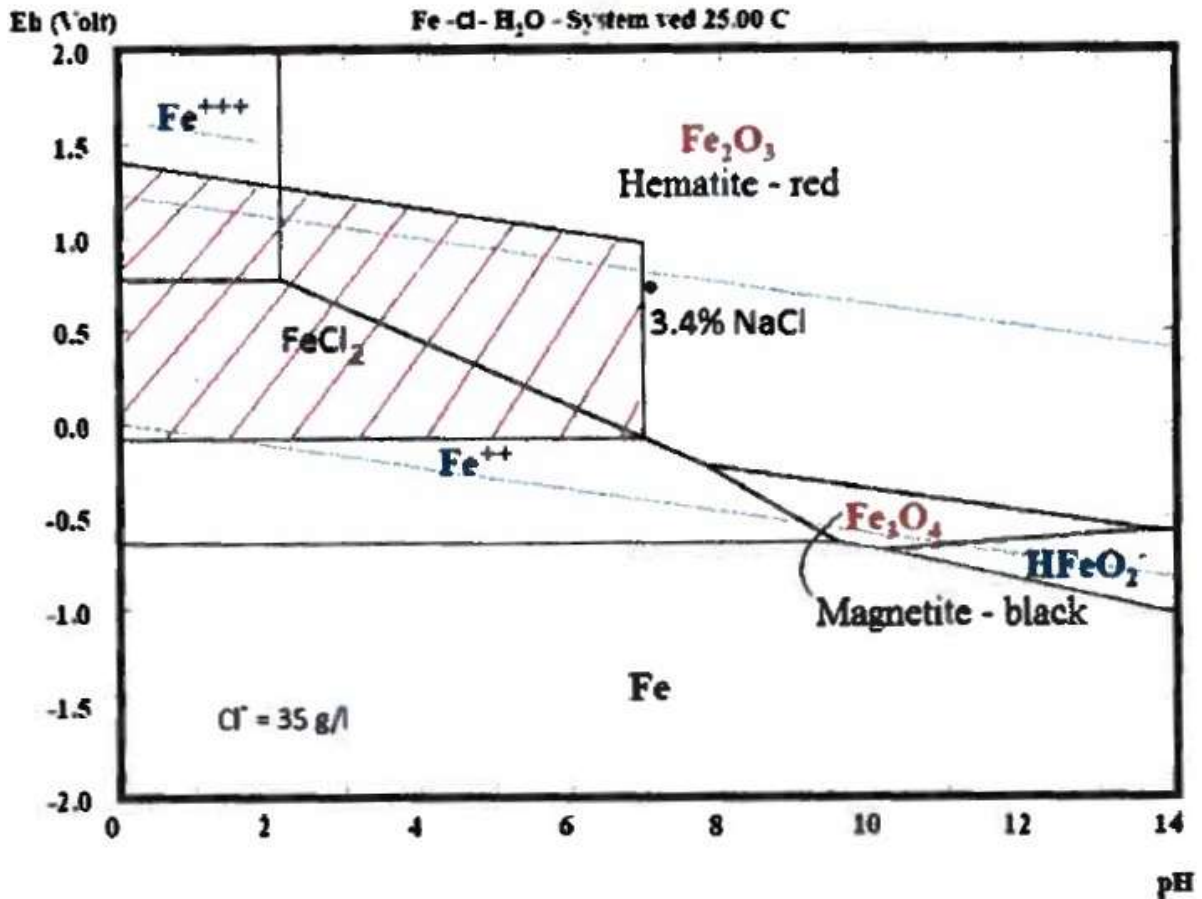
Figure 22 Pourbaix diagram for iron in 3.5 wt. % NaCl at 25° C [13].

It is presumed that the activity of the ferrous ions is $a_{Fe2+}=10^{-6}$, which is assumed to be realistic lower value for corrosion of practical significance [11].

From reaction a) it is seen that the equilibrium potential increases with increased iron ion activity. If the potential is increased to a value above the ion activity (10^{-6}), the system will try to restore the equilibrium. This can only happen by an increase of Fe^{2+}, i.e. corrosion [11].

The oxidised state of the material is when the potential is above the lines b),c) and d). Above these lines the oxides produced creates a diffusion barrier, making the surface passivated [11].

When the potential is below the lines a) and b), the metal state Fe is stable. Consequently, the metal is immune to corrosion in this area [11].

3.3.3 Polarisation

During polarisation the potential for the electrode reactions are shifted from equilibrium due to a net electrode reaction, i.e. a net current is flowing through the interface between metal and liquid. A way to measure the polarisation is over potential, which is the difference between the real potential and the equilibrium potential. When corrosion occurs on a surface, the real potential has to be between the equilibrium potentials for the anodic and cathodic reactions, see Figure 23 [11].

Equilibrium potential for cathodic reaction $= E_{oc}$

Equilibrium potential for anodic reaction $= E_{oa}$

Real potential $= E$

Cathodic overvoltage $= \eta_c = E - E_{oc} < 0$

Anodic overvoltage $= \eta_a = E - E_{oa} > 0$
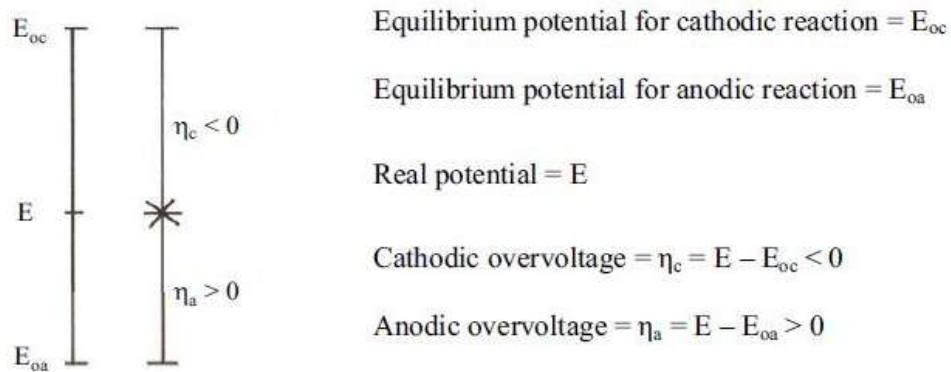
Figure 23 Equilibrium potentials, real potential and overvoltage [11].

It is possible to determine the corrosion rate of a metal by utilizing polarisation curves. This can be done with a potentiostat, see Figure 24. A potentiostat is an apparatus that holds a set electrode potential over the working electrode-reference electrode cell, and delivers the current demanded to keep it [11].
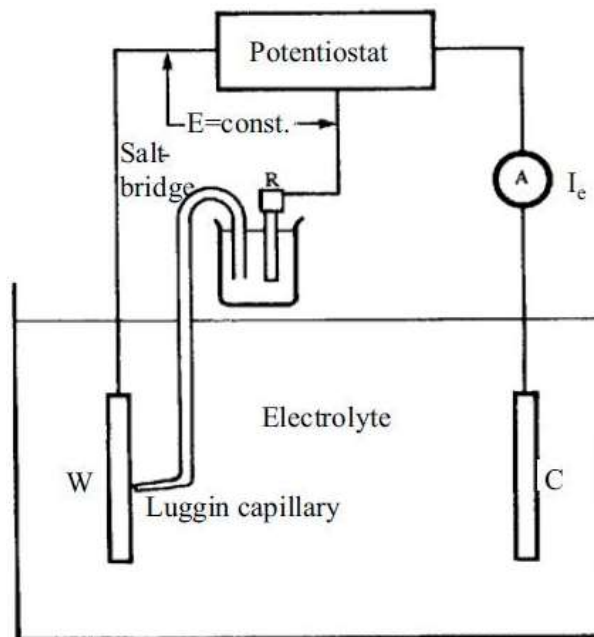
Figure 24 Wiring diagram for potentiostatic experiments [11].

Where:

W   is the work electrode (the sample examined).

C   is the counter electrode.

R   is the reference electrode.

It is assumed that only two reactions can occur on the working electrode, in accordance with the over potential curves and corrosion potential (E_{corr}) shown in Figure 25.
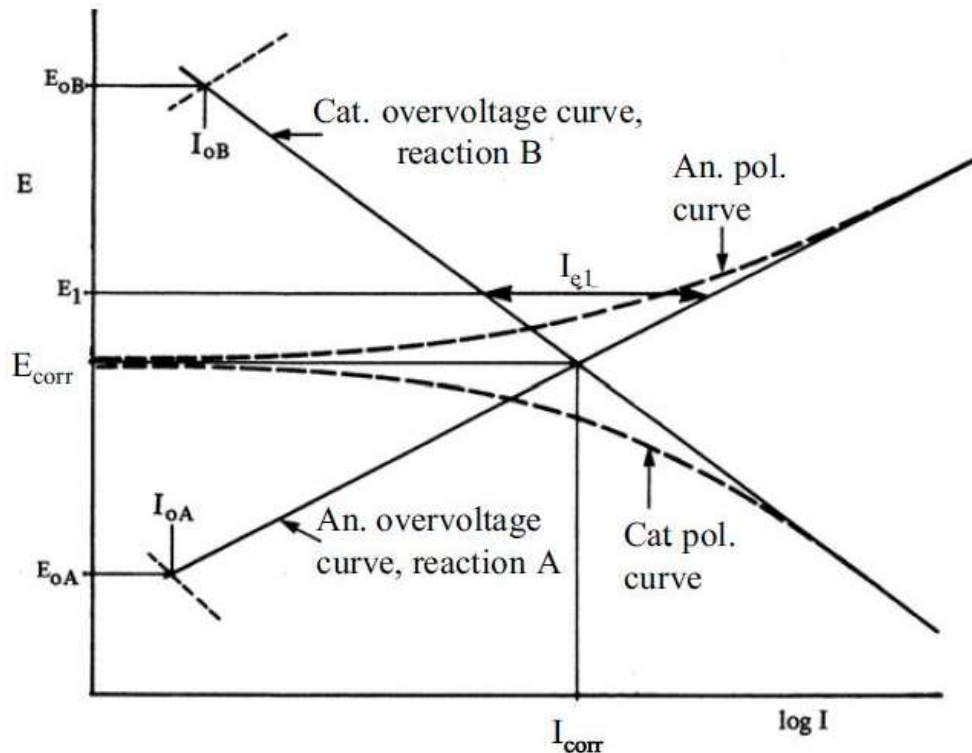

Figure 25 Overvoltage curves and corresponding polarization curves [11].

When $E = E_{corr}$, no current is feed from the potentiostat to the working electrode. However, if the potentiostat is set to an arbitrary potential (E_1) a current (I_{y1}) will be delivered. The current delivered is the difference between anodic and cathodic reaction current at this potential. When plotting the logarithm of the delivered current as a function of the potential, we obtain a polarisation curve as the one shown in Figure 25 [11].

3.3.4 Tribocorrosion

Tribocorrosion is material deterioration or transformation as a result of simultaneous action of wear and corrosion [14].

Most of the theory on tribocorrosion is about passive metals. A passive metal is a metal where the surface oxidizes, forming a thin film that protects the base material from further oxidation according to Equation 26 [14]:

$$M + nH_2O \rightarrow MO_n + 2nH^+ + 2ne^- \qquad \text{Equation 26 [14].}$$
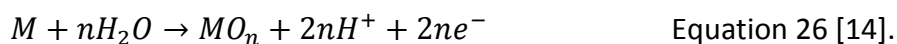
Where M represents a metal and n is the number of electrons transferred.

When a passive metal exposed to a corrosive electrolyte is rubbed against a solid, both corrosion and wear occur. Depending on how severe the wear is, rubbing will cause the film to become thinner or completely removed. Depending on the solution the passive film may or may not be restored. If the passive film is not restored, galvanic current will start to flow between the wear scar and the undamaged surface. In the wear scar the anodic reaction will mainly occur and the cathodic reaction on the outside surface [15].

However, the steel used in this thesis is an active metal, i.e. it does not form a passive layer at pHs lower than 8 and reacts accordingly to Equation 14. In this case the passive film is replaced with corrosion products ($Fe(OH)_3$) causing a lower corrosion rate as described in the chapter above. The corrosion mechanisms are described in the "Corrosion mechanisms" chapter above. In addition the corrosion product may cause abrasive wear in accordance with the Wear mechanisms chapter.

3.4 Metallurgy

Metals can consist of several different crystal systems (e.g. BCC, FCC and HCP) and structural elements. A schematic representation is shown in Figure 26 [16].
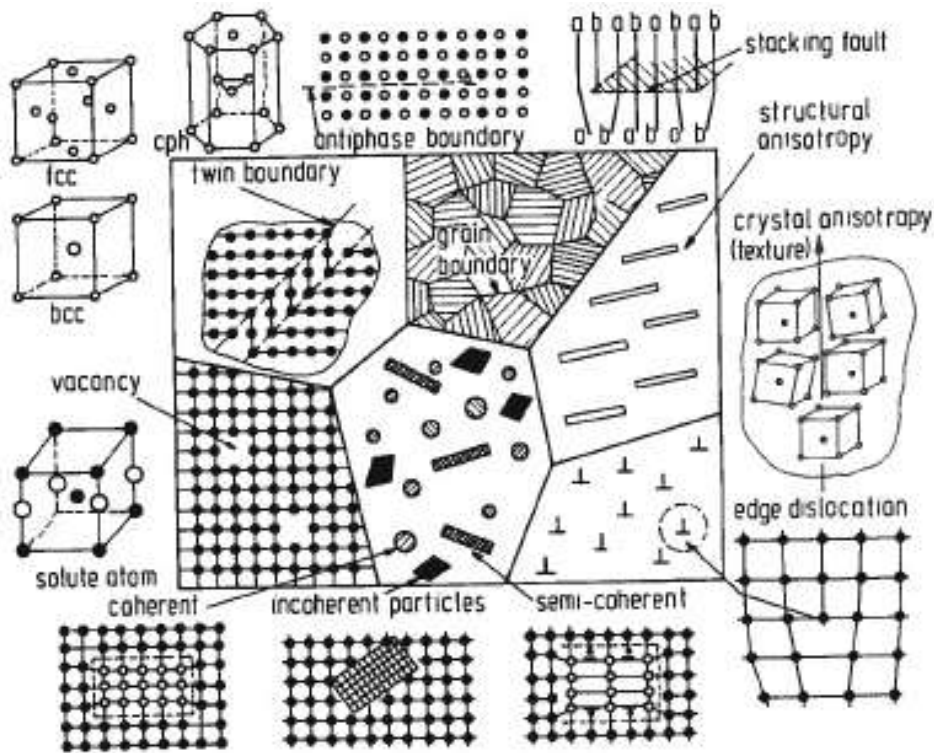
Figure 26 Schematic representation of strutural elements of inorganic solids [16].

The metal´s properties are among other determined by the size, shape and orientation, or chemical composition of the grains (crystals). In addition it is also dependent on the density of crystal defects (e.g. vacancies) or dislocations and the type, volume, size, shape or orientation of second phases (e.g. precipitated particles). Another factor influencing the microstructure of metal is the production method. The microstructure of the product can be altered by cold working (e.g. rolling), heat treatment (e.g. tempering) or a combination of these. Figure 27 shows an overview of the factors influencing the microstructure of a metal [16].
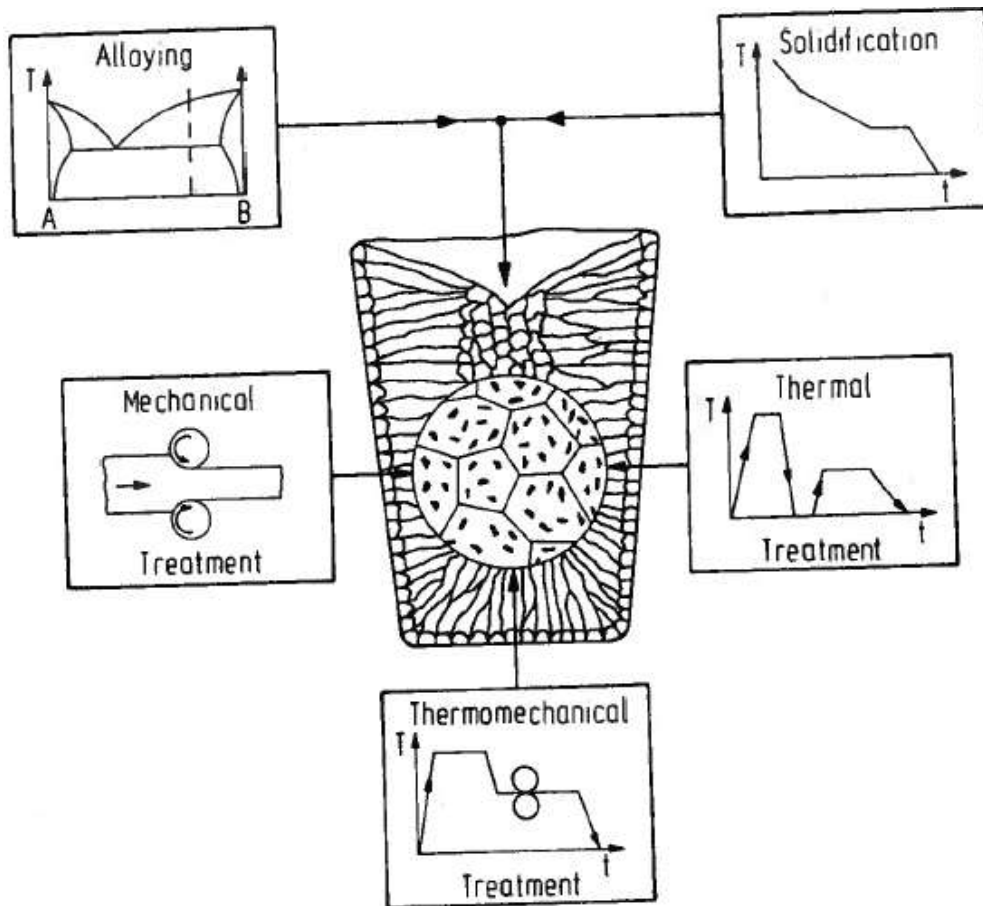
Figure 27 Schematic overview of different parameters which inflluence the microstructure [16].

Because the steel cutters used in the TBM are exposed to high forces and abrasive surfaces, the steel has to be able to withstand tough working conditions. This requires that the steel has a structure that gives high strength. However, it is important that the strength is not too high since this may cause it to become brittle. Steel with martensitic structures are often used for components exposed to rolling or rolling-sliding contacts, which is the contact scenario for TBMs [16].

Earlier studies have shown that the abrasive wear resistance of iron alloys increase with increasing carbon content. This may, among other, be due to the increasing work hardening capability of austenite or increasing hardness of martensite. Figure 28 shows the abrasive wear loss of iron alloys as a function of carbon content. However, it is important to remember that the wear loss at a given carbon content can differ considerable due to the microstructure of the alloy [16].
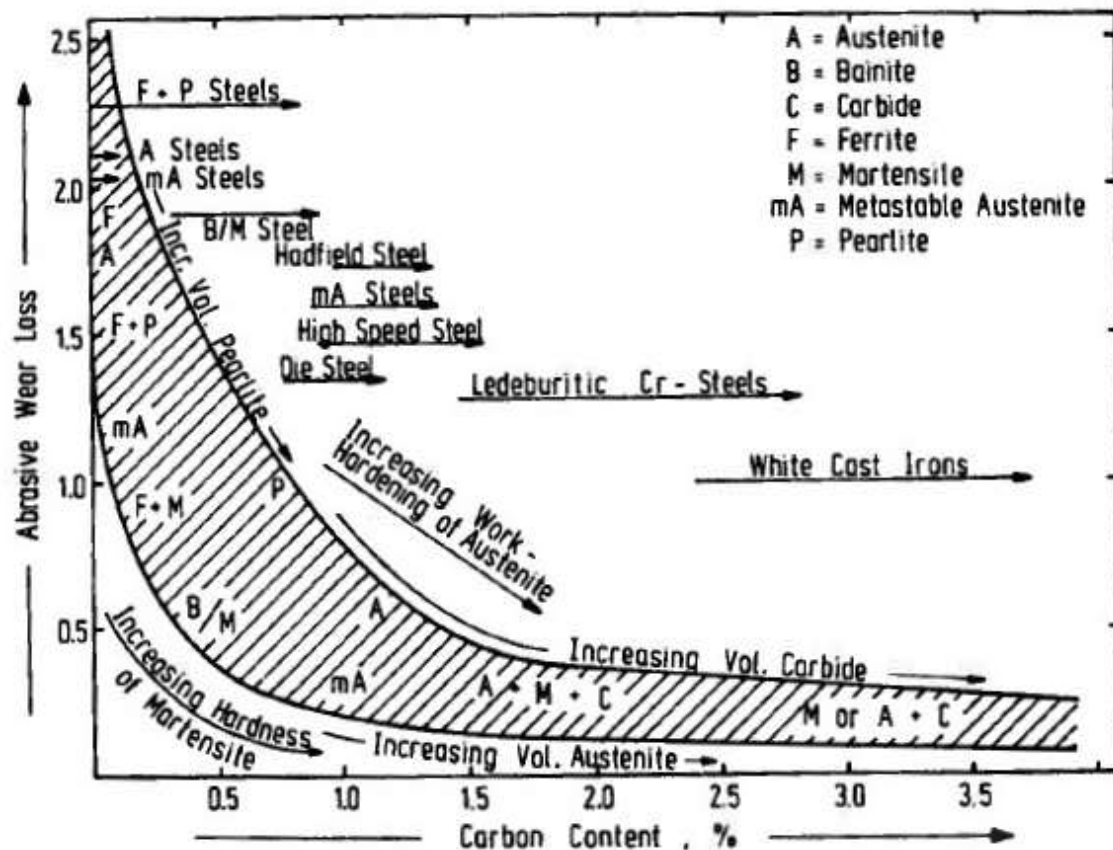
Figure 28 Abrasive wear loss of iron alloys measured by using a pin abrasion test versus carbon content of different Fe-alloys [16].

The abrasive wear loss has been shown to be strongly dependent on the carbon content within the range from 0 to about 0.8%. When the carbon content is above 0.8% the decrease in abrasive wear loss flattens out. Figure 29 shows an example of how dependent the abrasive wear loss is on the carbon content for carburized and hardened steel by use of a pin abrasion test. The carburizing has caused the carbon content of the steel to increase inwards from the surface. Due to the decrease of carbon content with increasing depth below the surface, the hardness of the martensitic steel will also decrease. Consequently, the abrasive wear loss increases with increasing depth below the carburized surface [16].
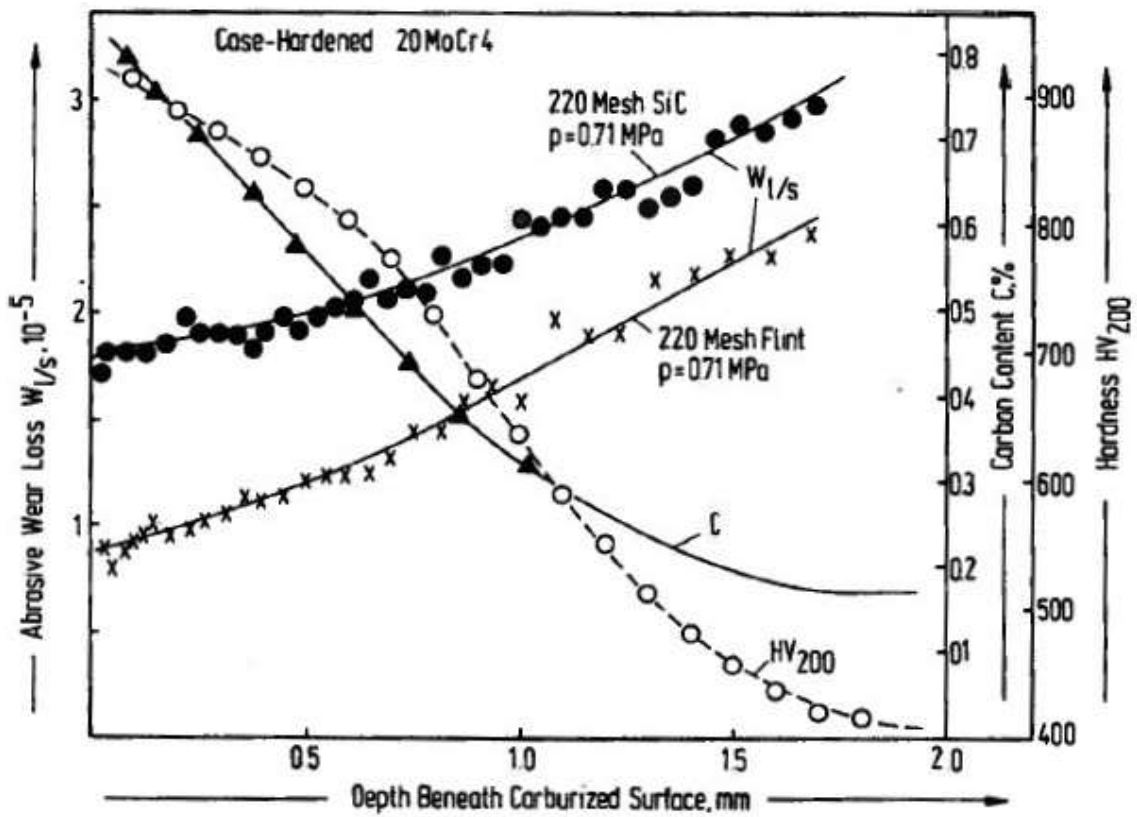
Figure 29 Abrasive wear loss measured by a pin abrasion test, carbon content and hardness of a carburized steel, as a function of depth below the carburized surface [16].

Although retained austenite (RA) may increase the work hardening capability, it can also cause spalling if the content of RA exceeds a certain value. Figure 30 shows how the mass loss and area of pitting is affected by %RA as a function of revolutions in a marginally lubricated rolling-sliding test [16].
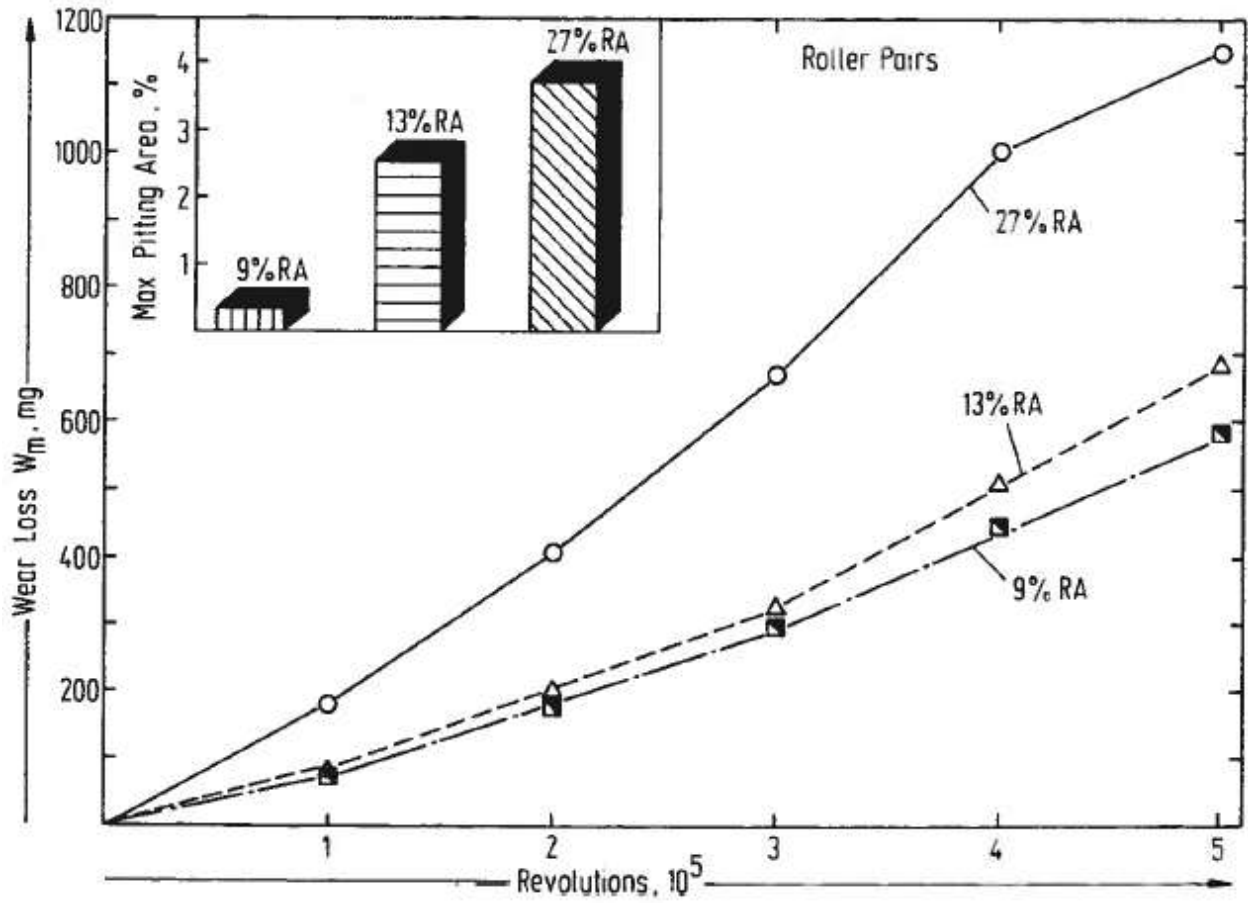
Figure 30 Mass loss and maximum area of pitting of steel containing different amounts of retained austenite, as a function of revolutions [16].

4 Experimental setup

4.1 Titration

To determine the amount of chloride in the water samples obtained from the field trips, precipitation titration was carried out. The test setup is shown in Figure 31.

The titration method used determines the amount of chloride ions by adding a $AgNO_3$ (silver nitrate) solution. The $AgNO_3$ solution is slowly added to the samples, forming a white silver chloride precipitate (Figure 32) according to Equation 27.

$$Ag^+_{(aq)} + Cl^-_{(aq)} \rightarrow AgCl_{(s)} \quad \text{Equation 27.}$$
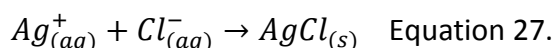
To determine when all the chloride ions have reacted to silver chloride, a K_2CrO_4 (potassium chromate) solution was added to the sample. This caused any excess $AgNO_3$ added to react with the K_2CrO_4, forming a red Ag_2CrO_4 precipitate (Figure 33) according to Equation 28.

$$2Ag^+_{(aq)} + CrO_4^{2-}{}_{(aq)} \rightarrow Ag_2CrO_{4\ (s)} \quad \text{Equation 28.}$$
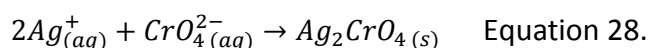
In order to make sure that all the chloride reacted, the solution was stirred by a magnetic stirrer.

When the amount of $AgNO_3$ needed to react with the chloride was found. The concentration of chloride was calculated by using Equation 29 and Equation 30.

$$C = \frac{n}{V} \qquad \text{Equation 29.}$$

$$M_W = \frac{m}{n} \qquad \text{Equation 30.}$$

Where M_W is the molar weight, m is the weight, n is the number of moles, C is the concentration and V is the volume.

Figure 31 Titration setup.

Figure 32 Solution with white AgCl precipitate.

Figure 33 Solution with red Ag2CrO4 precipitate.

4.2 Steel characterisation

In order to characterise the properties of the steel ball, a sample was polished and etched to take a picture of the microstructure in an optical microscope, the hardness was measured and an XRF-analyse (X-ray Fluorescence) was conducted by a hand held unit. The hardness measurement and XRF-analyse was done on a STRUERS Duramin-A2500 and a Niton XL3t XRF Analyzer, respectively. The hardness value was based on measurements from six different areas of the cutter cross-section, see Figure 34. At each area four measurements were made with a 3 mm distance between each other, except for area 1, where the distance was 1, 5 mm.
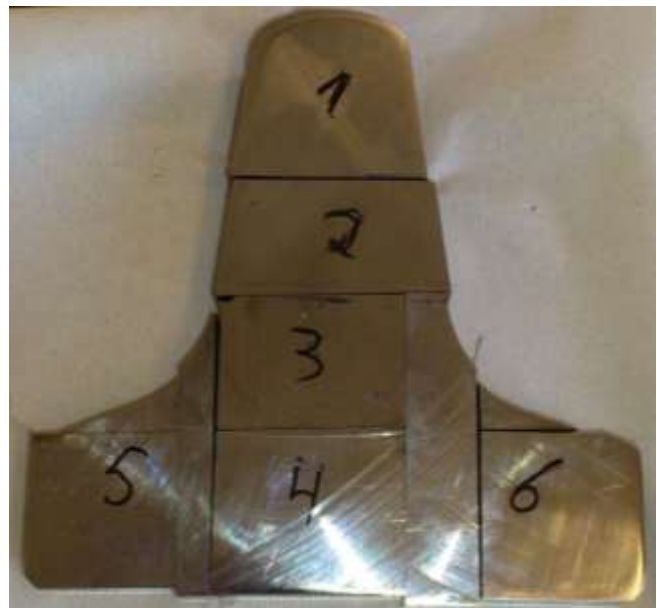
Figure 34 Cross-section of cutter tool with the hardness measurement areas.

4.3 Rock and Soil characterisation

In order to characterise the rocks and the soil used in this master thesis both XRD and SEM was used. Both the rock and the soil mineralogy were determined by an XRD-analysis and in addition the soil was investigated in a SEM. The SEM pictures taken of the soil was further analysed with software named ImageJ [17]. This software characterised the geometrical properties of the particles in the soil. The XRD-analyse and SEM pictures was performed on a Bruker D8 ADVANCE DIFFRAC^{plus} SEARCH and a Hitachi S-3400N, respectively. The rock and soil characterised were obtained from on-going tunnel borings sites in the Faroe Islands and Israel, respectively.

4.4 Test procedure

For this thesis it is assumed that the water is saturated with air at room temperature.

4.4.1 Polarisation curves

In order to determine the polarisation curves of the steel used in this master thesis, a potentiostat was used (Figure 35 and Figure 36). The polarisation curves were obtained by applying voltage ±700 mV from the E_{corr} and with a speed of 5 mV each second, both in the anodic and cathodic areas. The potentiostat and software used in this test were AUTOLAB and Nova version 1.5, respectively.
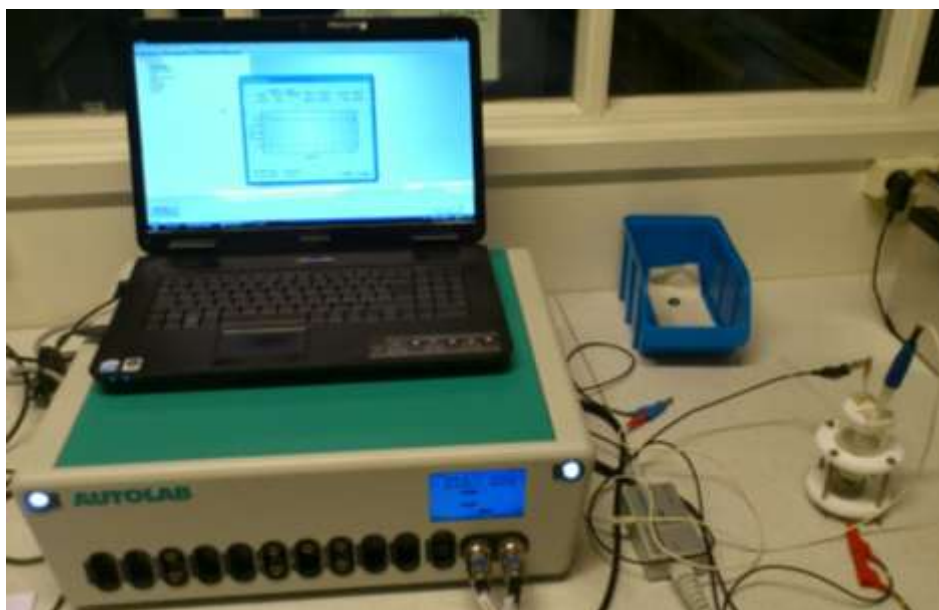
Figure 35 The potentiostat used in this master thesis.

Figure 36 The cell setup used in this master thesis.

4.4.2 Reciprocal ball-on-plate

The test rig used to determine the abrasion-corrosion properties of the cutter steel was a ResMat Tribocorr, Figure 37. The test was performed by sliding a steel ball back and forth with a stroke length of 10 mm, see Figure 38. During the tests rocks obtained from a tunnel boring site at the Faroe Islands were exposed to dry conditions, liquid solutions obtained from the same site as the rock samples and a mixture of 50 vol.% of the liquid solution and 50 vol.% foam additive. The foam used was MEYCO ABR 5 [18]. This foam is used in rock tunnelling. The water used had a pH value of 7.7.

Figure 37 ResMat Tribocorr.
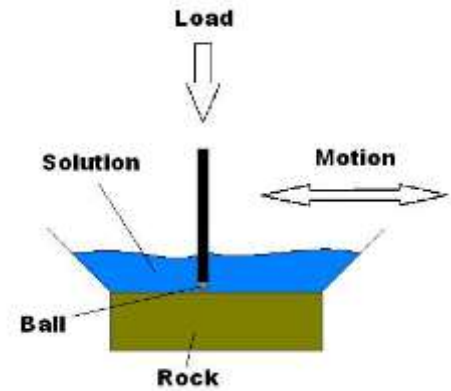
Figure 38 Test course of the ball holder on the rock.

During each test the friction coefficient between the substrate and steel ball was measured. The balls were cleaned in alcohol in an ultrasonic bath before the weight loss of the steel ball using a METTLER AT400 weight capable to measure weight differences of 0. 1 mg.

After the tests were performed, the wear present on the cutter balls and rock specimens were examined in a Scanning Electron Microscope (SEM). In order to be able to see the rocks in the SEM, they had to be sputtered with carbon. The SEM pictures were taken on a Hitachi S-3400N. In addition, the solutions in which the tests were performed were sent to an ICP analysis to determine the iron (Fe), copper (Cu), nickel (Ni) and chromium (Cr) content.

4.4.3 Rubber Wheel

To test the abrasivity of the soils, a Rubber Wheel test rig was used (Figure 39 and Figure 40). The tests are performed by applying a force of 220N between the rubber wheel and the specimen, and rotating the rubber wheel. The rubber wheel has a durometer hardness of 70 and rotating at about 200 revolutions per minute (rpm). The rubber wheel diameter is 7 inches, consequently, a rotating speed of 200 rpm is equivalent to about 2 $^m/_s$, which is within the range of what a cutter disc may be exposed to during boring.

Figure 39 Picture of the Rubber Wheel test setup used.
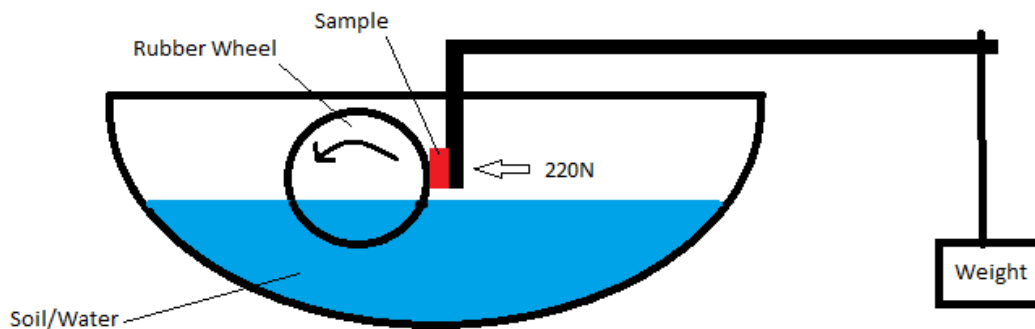
Figure 40 Sketch of the Rubber Wheel test setup.

Four different solutions were tested:

- Sand and water from Israel (Israel S&W).
- Casting sand and water from Israel (C-sand & I-water).
- Sand and water from Israel + Foam additive (Israel S&W + Foam).
- Sand and water from Israel + Oil (Israel S&W + Oil).
- Casting sand and water from the Faroe Islands (C-sand & F-water).

The water from Israel and Faroe Islands had a measured pH value of 8.1 and 7.7, respectively. The foam additive and oil used was MEYCO SLF41 [19] with a measured pH-value of 3.3 and Shell Tellus S 32 [20], respectively. The abrasive value (SAT) of the sand from Israel and casting sand was 20 and 21, respectively.

Each test lasted for a total of 60 minutes and the sample was cleaned in alcohol and an ultrasonic bath and weighted every 10 minutes during the test. The weighting of the samples were conducted on a METTLER AT400 weight capable to measure weight differences of 0. 1 mg. After the tests were performed, the wear present on the sample surfaces were examined in a SEM (Hitachi S-3400N). In addition, the solutions in which the tests were performed were sent to an ICP analysis to determine the Fe, Cu, Ni and Cr content.

The roughness on the surface of the samples used was measured to an average of 0.03 μm and 0.04 μm for R_a and R_q, respectively.

4.4.4 Hyperbaric Soil Abrasion test

The Hyperbaric Soil Abrasion Test is a new method under testing that simulates wear occurring during tunnel boring in soil. The test is performed by rotating two square steel rods perpendicular to each other in a container with a mixture of soil and water, or soil only. Figure 41 shows a picture of the test setup.

In this master thesis two conditions were tested:

- Soil saturated with water from Israel.
- Dry sand.

Both the soil and water used in this experiment were collected at a tunnel boring site in Israel.

Each test had a duration of 35-38 minutes and having a total boring length of 400mm.
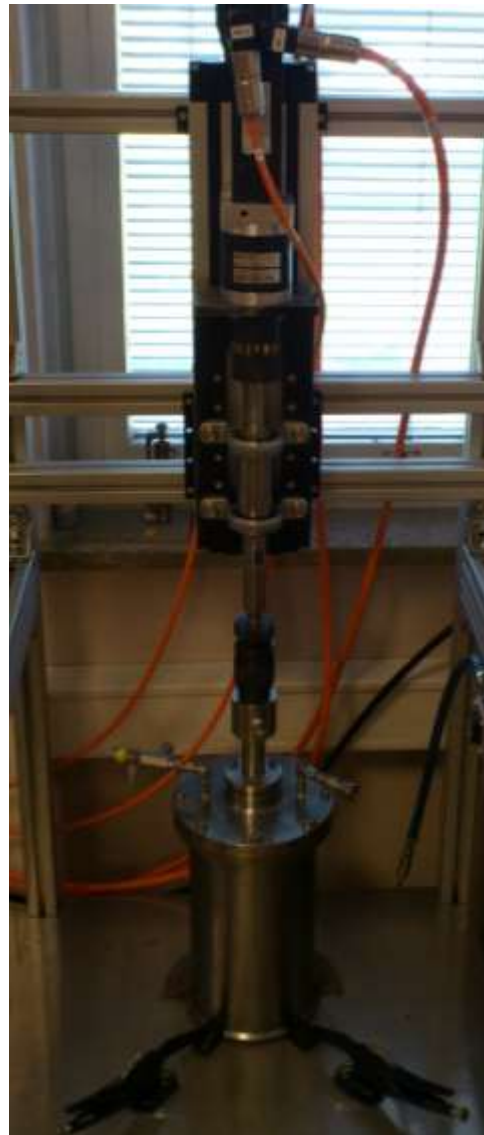
Figure 41 Test setup for the Hyperbaric Soil Abrasion Test.

5 Results

5.1 Chloride content

Below it is shown in Equation 31 to Equation 33 how to calculate the amount of chloride in a solution by titration with a $AgNO_3$ solution.

The first step is to determine how many moles (n) of $AgNO_3$ is needed to react with the chloride present, in accordance to Equation 27. To do this it is necessary to rearrange Equation 29 to the equation below:

$$n = C \cdot V \qquad \qquad \text{Equation 31.}$$

Where: C = [mol/L]
            V = [L]

The second step is to determine how many grams of chloride this is equivalent to. This is done by altering Equation 30 to the equation below:

$$m = M_w \cdot n \qquad \qquad \text{Equation 32.}$$

Where: M_w = [g/mol]
            n = [mol]

The last step is to determine the percentage share of chloride in the original test solution. The volume of the test solution was 100 mL, which is approximately 100g. Consequently, the equation for calculating the weight percent of chloride in the solution will be as shown below:

$$wt.\% = \frac{m_{Cl}}{100g} \cdot 100\% \qquad \text{Equation 33.}$$

Faroe Islands

Table 3 shows the amount of chloride present in the water sample from the Faroe Islands.

Table 3 Shows the amount of chloride present in the water from the Faroe Islands.

	Measurement 1	Measurement 2	Measurement 3
Volume $AgNO_3$ [mL]	3	5	6
n(Cl) [mmoles]	0.45	0.75	0.9
m(Cl)[g]	0.016	0.027	0.032
wt. %	0.02	0.03	0.03

This gives an average value of 0.02±0.01 wt. % chloride.

Israel

Table 4 shows the amount of chloride present in the water sample from Israel.

Table 4 the amount of chloride present in the water from Israel.

	Measurement 1	Measurement 2	Measurement 3
Volume $AgNO_3$ [mL]	27.1	26.8	27
n(Cl) [mmoles]	40.65	40.2	40.5
m(Cl)[g]	1.441	1.425	1.436
wt. %	1.44	1.43	1.44

This gives an average value of 1.43±0.01 wt. % chloride.

5.2 Steel characterisation

The optical microscope picture, see Figure 42, shows the microstructure of the steel ball. This is martensitic steel with some small areas of retained austenite structure. The hardness test showed that the hardness of the ball was 662±25 VHN.

The XRF-analysis showed that the composition of the additives in the steel ball was as shown in Table 5 below.
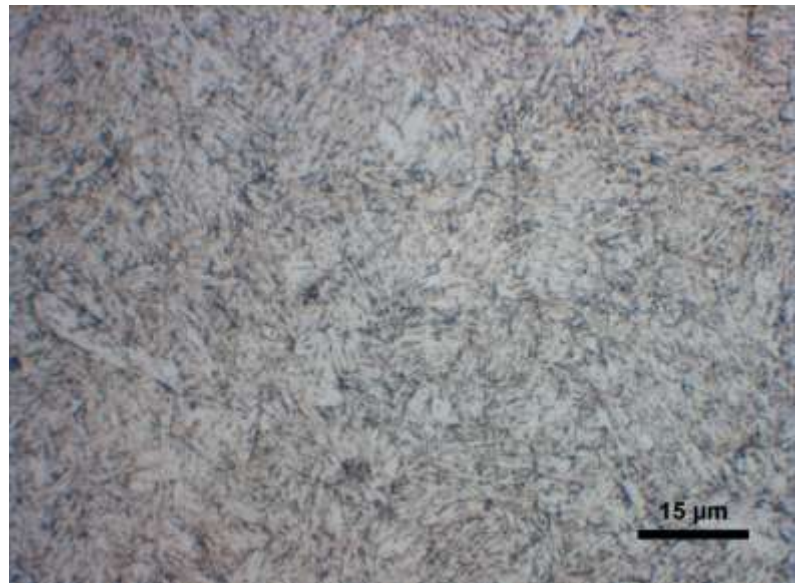
Figure 42 Picture of the microstructure taken in an optical microscope.

Table 5 Results from XRF-analysis of the steel.

Fe [%]	Cr [%]	Mo [%]	Si [%]	V [%]	Mn [%]	Ni [%]	Cu [%]	Ti [%]
90.14	5.26	1.28	1.19	1.02	0.23	0.14	0.04	0.02

5.3 Rock and Soil characterisation

5.3.1 Rock

The results from the XRD analysis of the rock showed that the main mineral present in were feldspar (Table 6).

Table 6 Results from XRD of rock sample from the Faroe Island.

Mineral group	Mineral	[wt.%]
Feldspar	Plagioclase	79
	K-feldspar	4
Pyroxene	Clinopyroxene	12
Quartz	Quartz	3
Spinel	Magnetite	2
Total		100

5.3.2 Soil

The results from the XRD analysis of the soil from Israel showed that the main mineral present were quartz (Table 7).

Table 7 Results from XRD of soil sample from Israel.

Mineral group	Mineral	[wt.%]
Quartz	Quartz	72
Calcite	Calcite	10
Feldspar	Plagioclase	10
	K-feldspar	6
Amphibole	Actinolite	2
Total		100

Figure 43 shows the SEM picture of the sand from Israel used to determine the shape of the particles by use of ImageJ. ImageJ marked the outlines of the particles (Figure 44) and calculated several shape descriptors. Figure 45, Figure 46 and Figure 47 shows that the Aspect Ratio, roundness and form factor, respectively, are spread over a wide range.
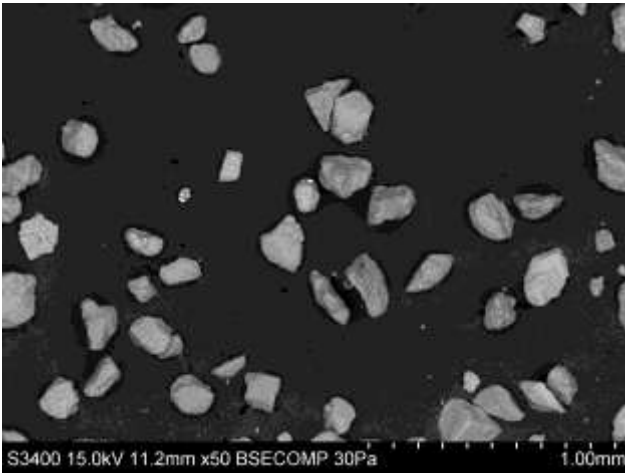
Figure 43 SEM picture of sand from Israel.

Figure 44 Outlines of the particles from a SEM picture, used for calculating shape descriptors in ImageJ.
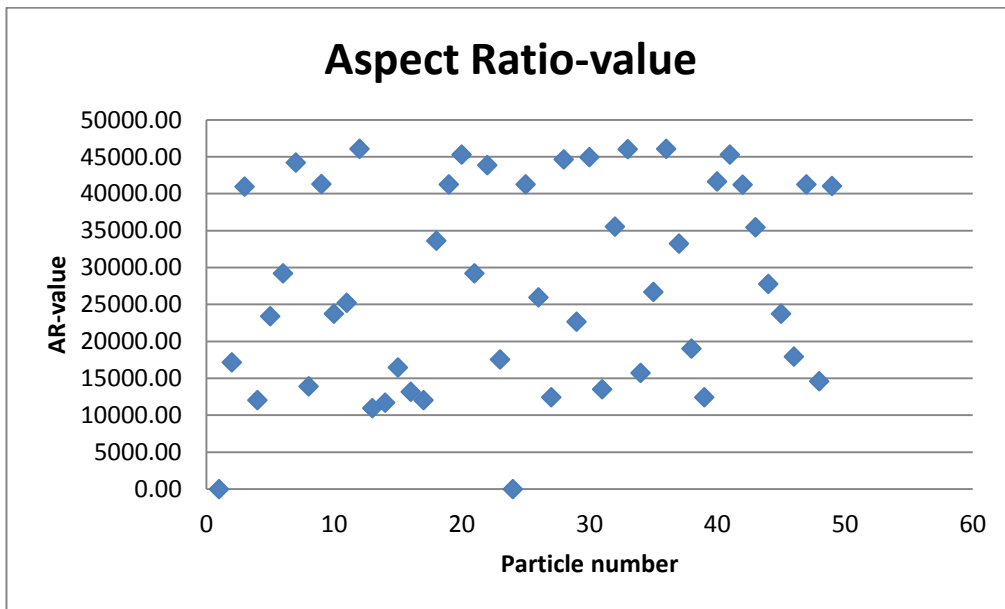
Figure 45 Aspect Ratio as a function of particle number.
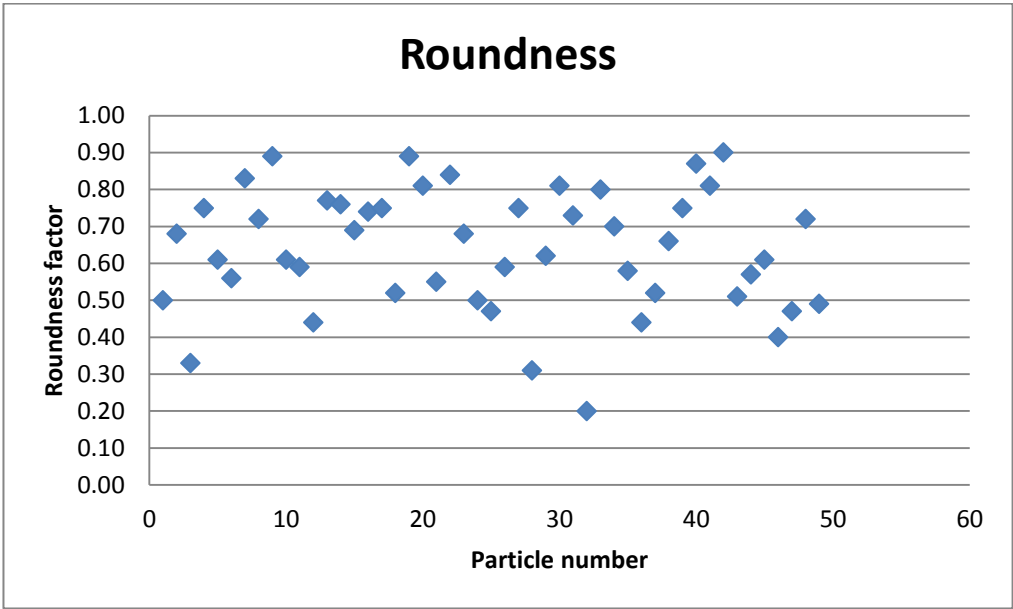
Figure 46 Roundness as a function of particle number.
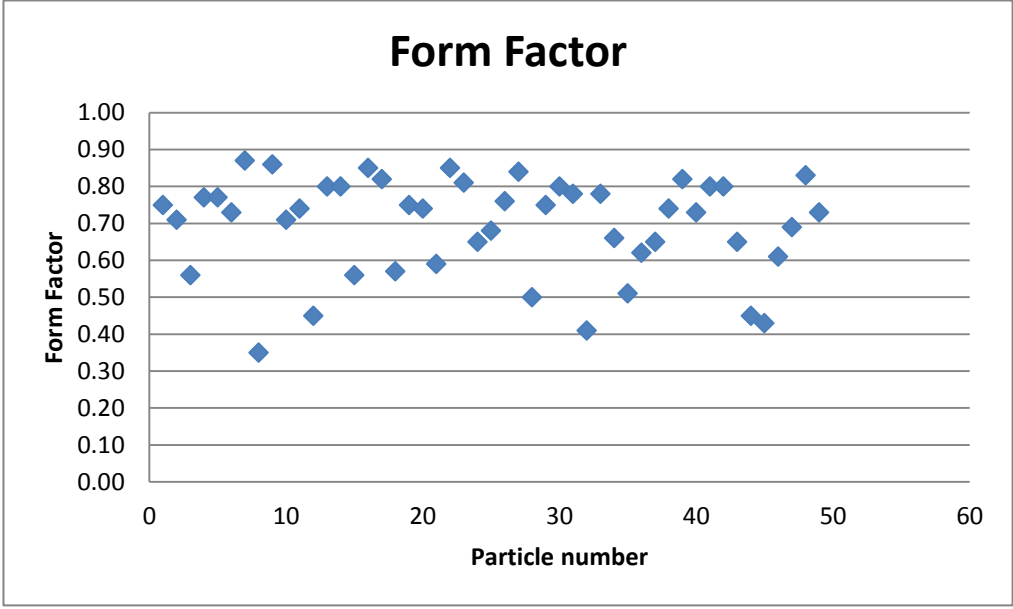
Figure 47 Form Factor as a function of particle number.

5.4 Polarisation

Figure 49 and Figure 47 show the polarisation curves for the water samples collected in the Faroe Islands and Israel, respectively. For the water sample from Israel the addition of foam did not alter the corrosion potential significantly. However, for the Faroe Island sample the foam caused a drop in corrosion potential at about 0.25 V.
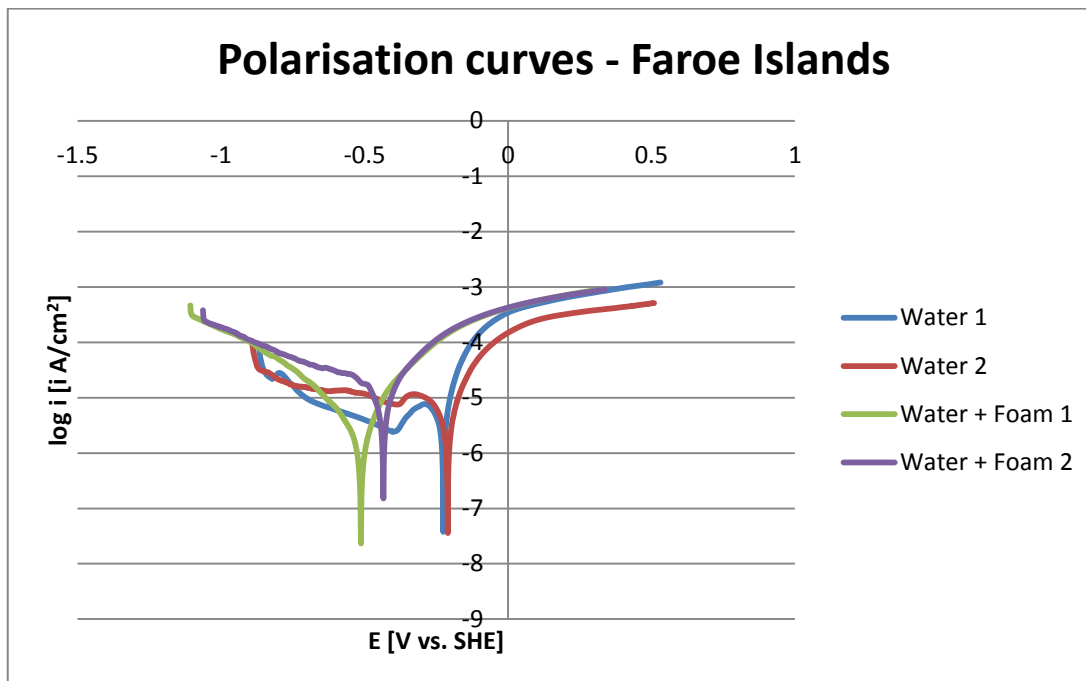
Figure 48 Polarisation curves for the water from the Faroe Islands.
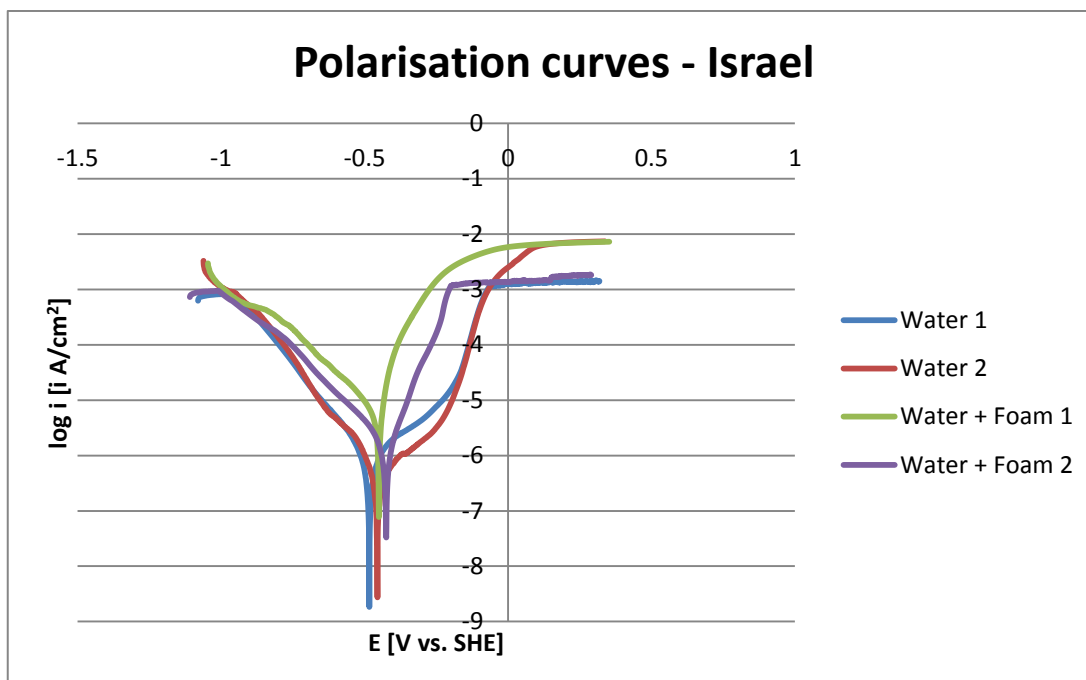
Figure 49 Polarisation curves for the water from Israel.

5.5 Corrosion-abrasion

5.5.1 Reciprocal ball-on-plate

Table 4shows the average coefficient of friction (COF) and weight loss on the steel ball during the reciprocal ball-on-plate test. Figure 50 to Figure 52 shows the variations in the COF during the three test scenarios.

Table 8 Average COF and weight loss for the reciprocal ball-on-plate test.

	Dry wear	Wet Wear	Lubricated wear
Average COF:	0.98 ±0.10	0.70 ±0.08	0.16 ±0.04
Average weight loss [g]:	0	0	0
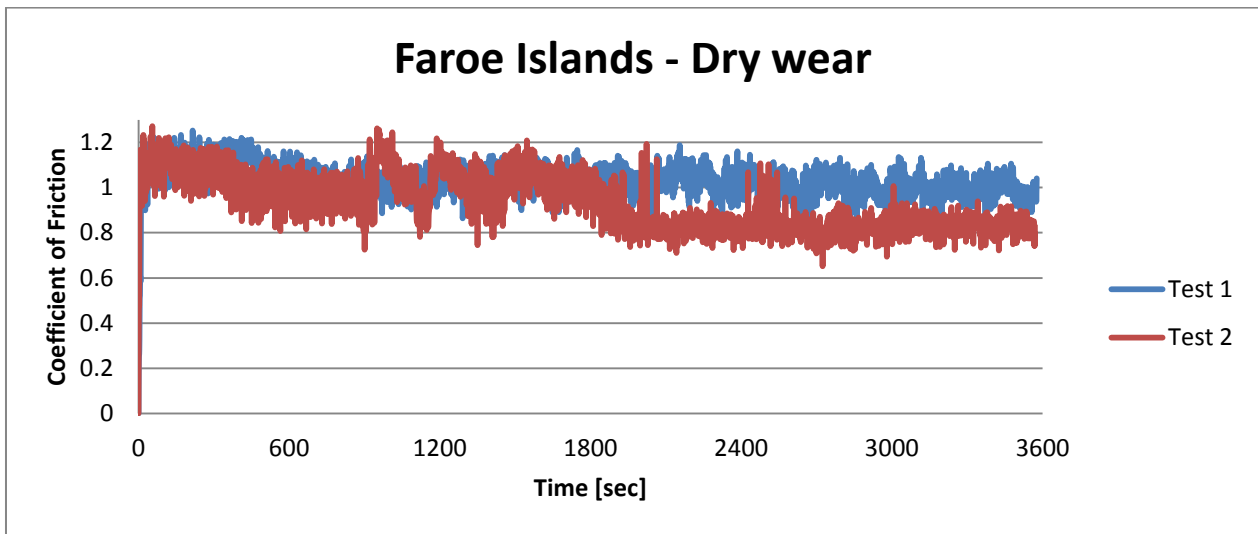
Figure 50 Friction coefficient graphs for dry rubbing steel ball on rock.
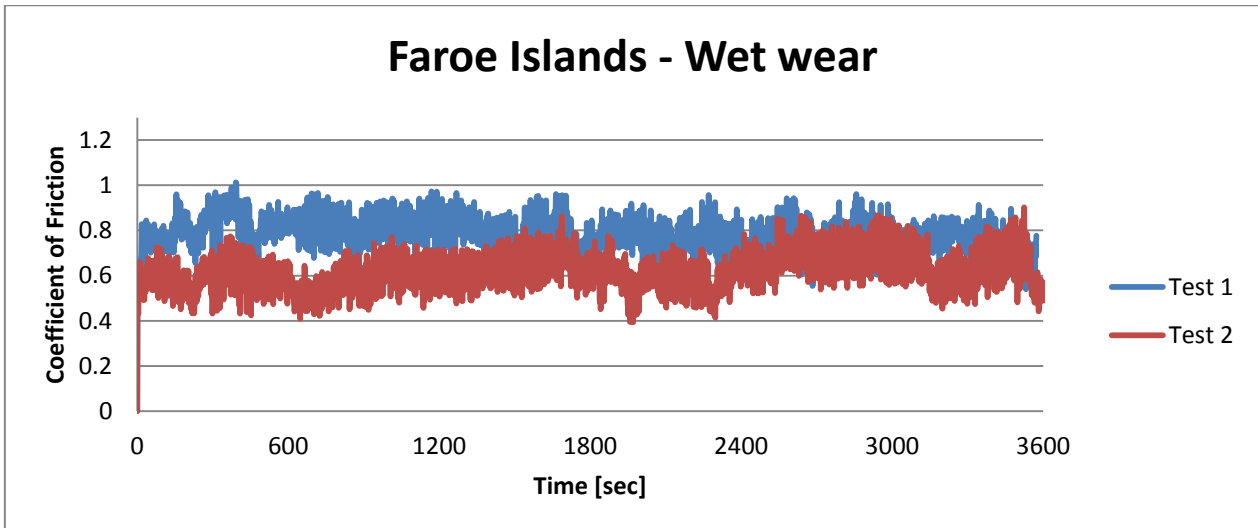
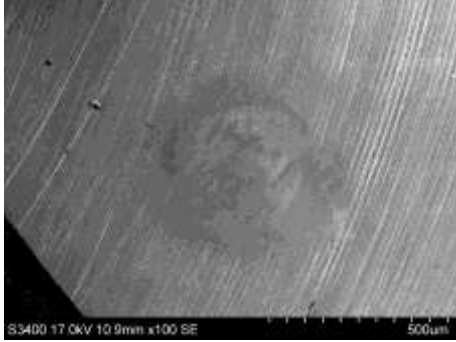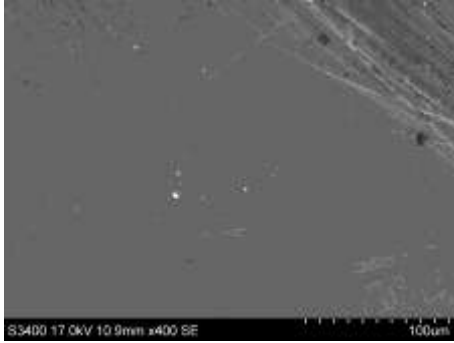**Figure 51 Friction coefficient graphs for wet rubbing, water lubricated, steel ball on rock.**
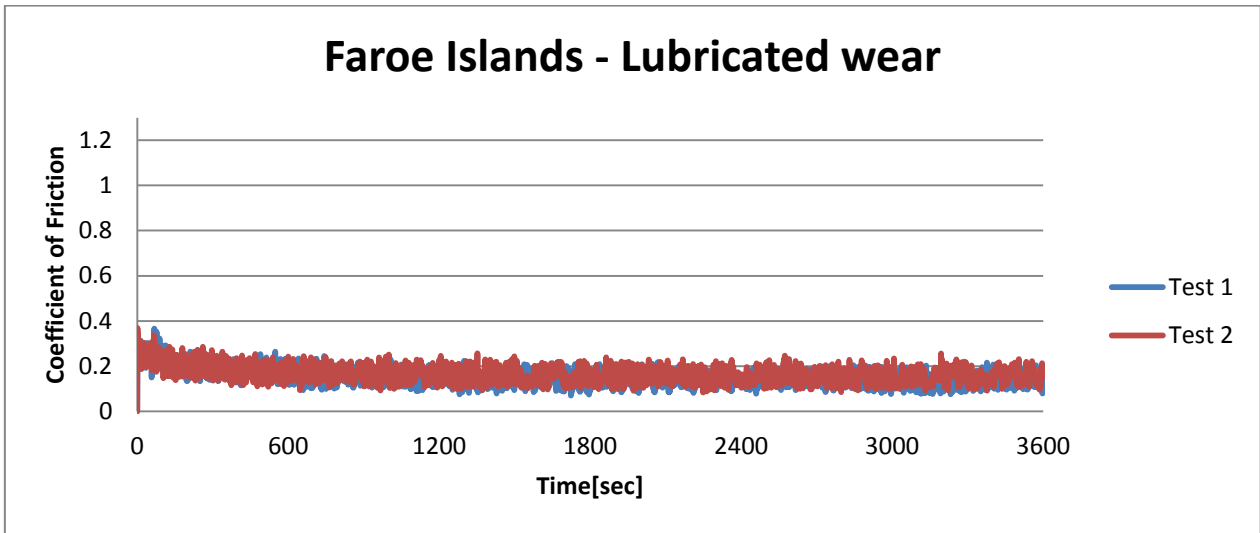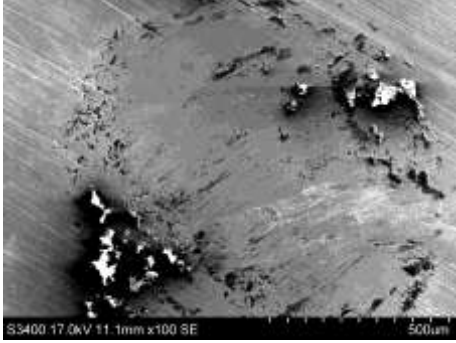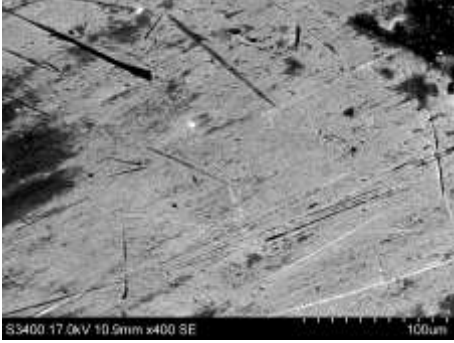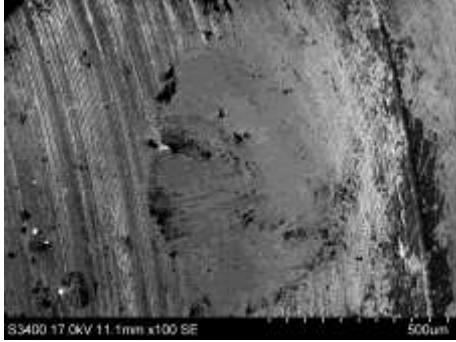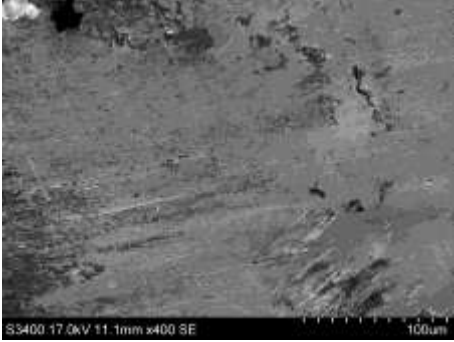
Figure 52 Friction coefficient graphs for lubricated rubbing steel ball on rock.

Wear on the steel balls

The wear occurring on the steel ball by rubbing on rock at dry, water lubricated and foam lubricated scenarios are presented in Figure 53 to Figure 58 (Table 9).
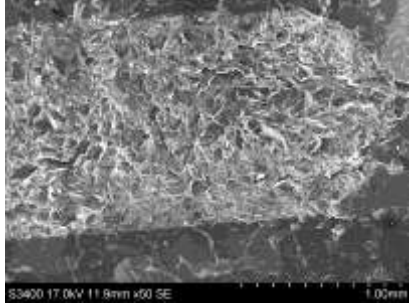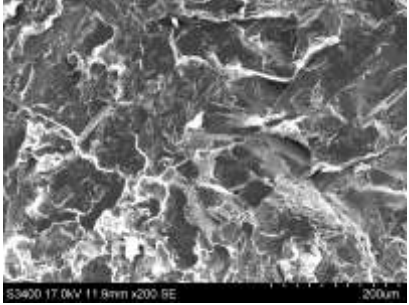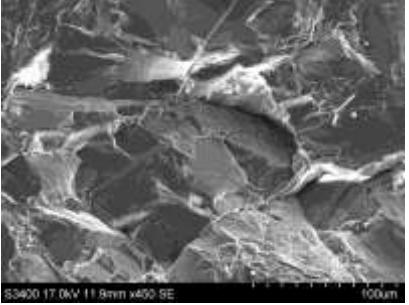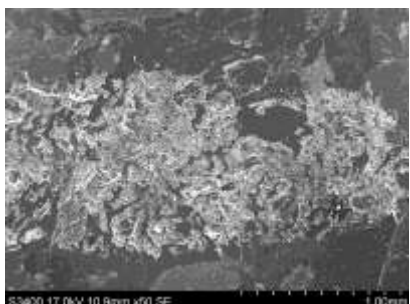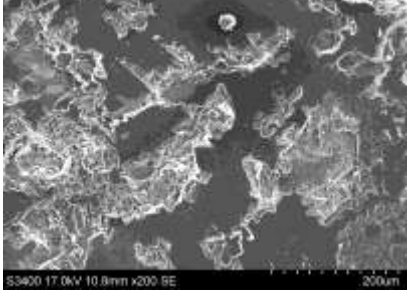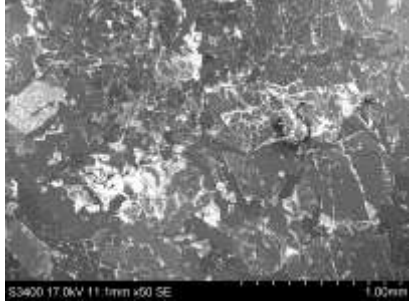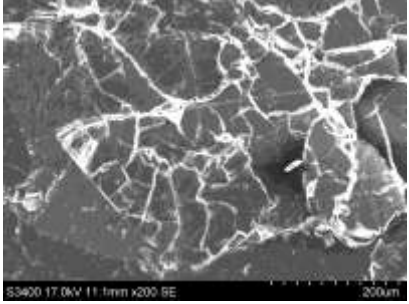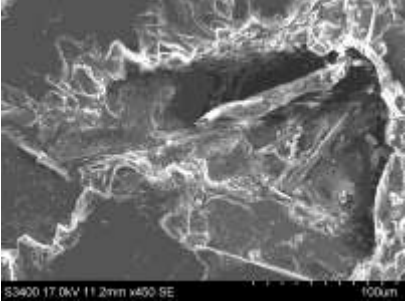
Table 9 SEM pictures of the steel surface after reciprocal ball-on-plate test.

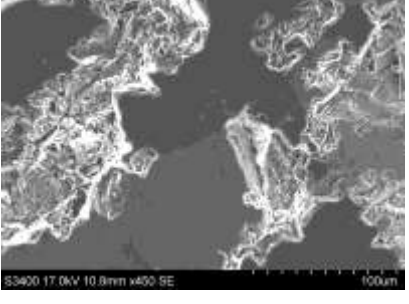| Condition	Magnification	
	100X	400X
Dry wear	**Figure 53 Wear track on the steel ball from dry wear at 100X magnification.**	**Figure 54 Wear track on the steel ball from dry wear at 400X magnification.**
Wet wear (water)	**Figure 55 Wear track on the steel ball from wet wear, lubricated with water, at 100X magnification.**	**Figure 56 Wear track on the steel ball from wet wear, lubricated with water, at 400X magnification.**
Lubricated wear (foam)	**Figure 57 Wear track on the steel ball from lubricated wear at 100X magnification.**	**Figure 58 Wear track on the steel ball from lubricated wear at 400X magnification.**

Wear on rocks

The wear that occurred on the rock surface by being rubbed upon by the steel ball at dry, water lubricated and foam lubricated scenarios are presented in Figure 59 to Figure 67 (Table 10).

Table 10 SEM pictures of the rocks.

Condition	Magnification		
	50X	200X	450X
Dry wear	Figure 59 Wear track on the rock from dry wear at 50X magnification.	Figure 60 Wear track on the rock from dry wear at 200X magnification.	Figure 61 Wear track on the rock from dry wear at 450X magnification.
Wet wear (water)	Figure 62 Wear track on the rock from wet wear, water lubricated, at 50X magnification.	Figure 63 Wear track on the rock from wet wear, water lubricated, at 200X magnification.	Figure 64 Wear track on the rock from wet wear, water lubricated, at 450X magnification.
Lubricated wear (foam)	Figure 65 Wear track on the rock from lubricated wear at 50X magnification.	Figure 66 Wear track on the rock from lubricated wear at 200X magnification.	Figure 67 Wear track on the rock from lubricated wear at 450X magnification.

IPC

The results from the IPC analysis showing the amount of chromium, iron, nickel and copper in the solutions from the reciprocal ball-on-plate test are presented in Table 11 and Figure 68. The concentrations shown in Figure 68 are in a logarithmic scale.

Table 11 Concentration of Cr, Fe, Ni and Cu in the test solutions used in the reciprocal ball-on-plate test.

| Condition	Cr [µg/L]	Fe [µg/L]	Ni [µg/L]	Cu [µg/L]
Faroe Island water	0.4219	2.7474	3.5440	5.0075
Faroe Island water + foam	47.6697	1231.1227	71.6108	37.5114
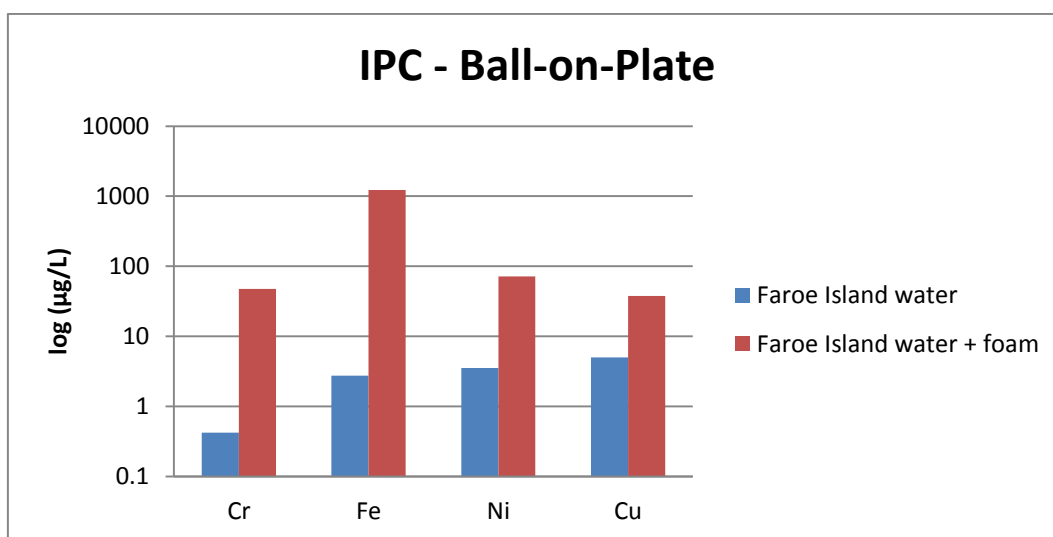
Figure 68 Graphical presentation of the results from the IPC analysis of the Ball-on-Plate test.

5.5.2 Rubber Wheel

The average weight loss of the steel samples from the rubber wheel test is shown in Table 12and is presented graphically in Figure 69. The weight loss measured during each test is shown in Appendix A.

Table 12 Average weight loss during the Rubber Wheel test.
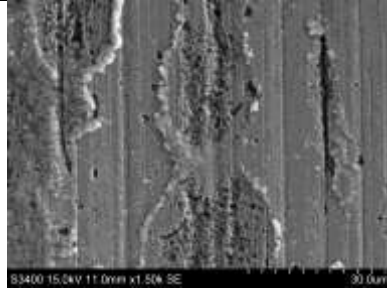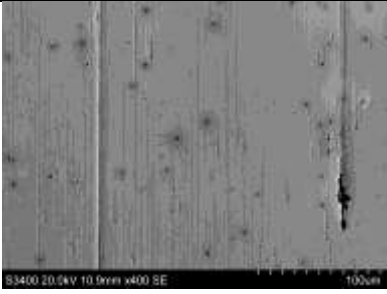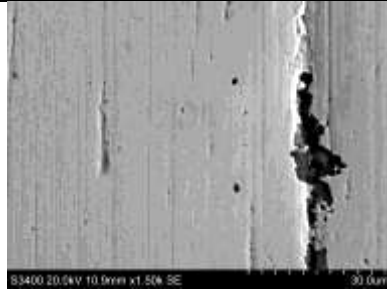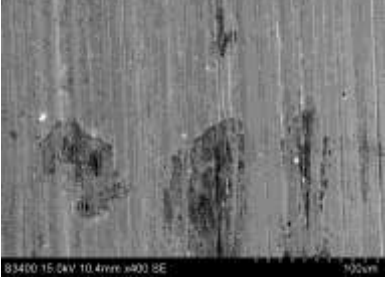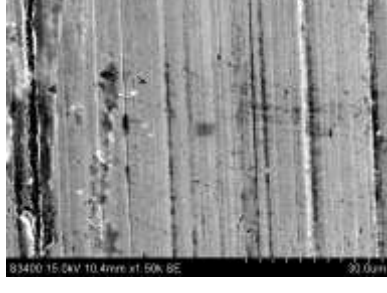
Condition	Average Weight loss [g]						
	0	10	20	30	40	50	60
				[minutes]			
Israel S&W	0.0000	0.0026	0.0165	0.0260	0.0350	0.0456	0.0577
C-sand & I-water	0.0000	0.0010	0.0052	0.0059	0.0068	0.0079	0.0089
C-sand & F-water	0.0000	0.0014	0.0022	0.0025	0.0029	0.0035	0.0038
Israel S&W + Foam	0.0000	0.0041	0.0079	0.0119	0.0154	0.0194	0.0234
Israel S&W + Oil	0.0000	0.0112	0.0257	0.0426	0.0592	0.0738	0.0908
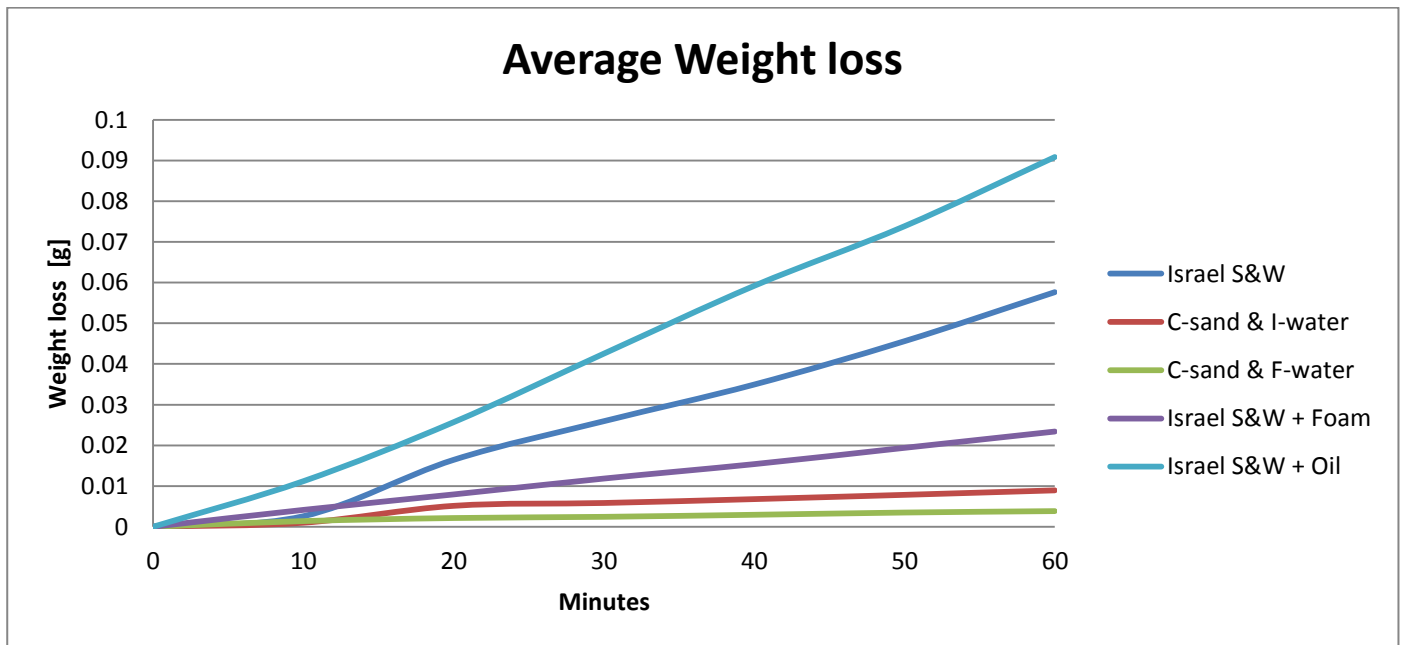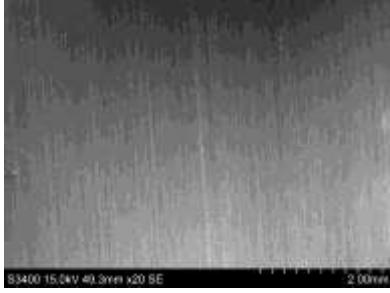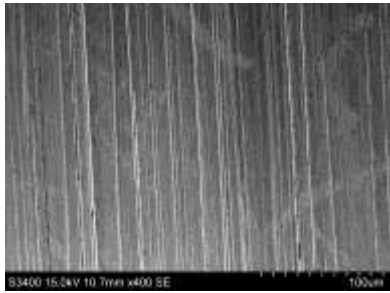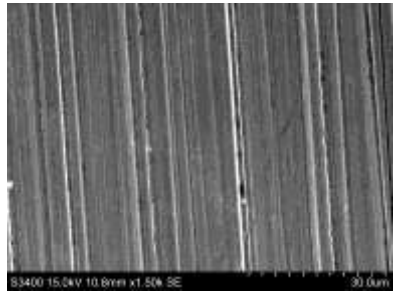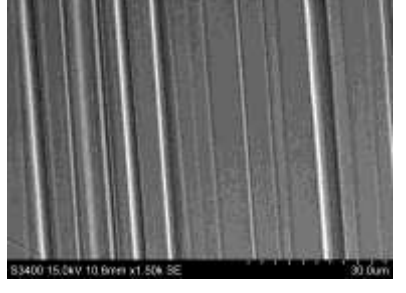
Figure 69 Average weight loss during the Rubber Wheel test.

The wear that occurred on the steel surface by the rubber wheel in the different sand, water and foam mixtures are presented in Figure 70 to Figure 84 (Table 13).

Table 13 SEM pictures of the steel surface after Rubber Wheel test.

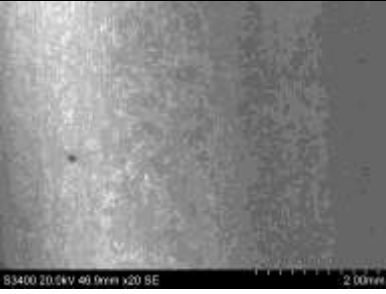| Condition	Magnification		
	20X	400X	1500X
Israel sand & water	**Figure 70 Wear track on the steel surface for Rubber Wheel test with sand and water from Israel at 20X magnification.**	**Figure 71 Wear track on the steel surface for Rubber Wheel test with sand and water from Israel at 400X magnification.**	**Figure 72 Wear track on the steel surface for Rubber Wheel test with sand and water from Israel at 1500X magnification.**
Israel sand & water + Foam	**Figure 73 Wear track on the steel surface for Rubber Wheel test with sand and water from Israel + foam additive at 20X magnification.**	**Figure 74 Wear track on the steel surface for Rubber Wheel test with sand and water from Israel + foam additive at 400X magnification.**	**Figure 75 Wear track on the steel surface for Rubber Wheel test with sand and water from Israel + foam additive at 1500X magnification.**
Israel sand & water + Oil	**Figure 76 Wear track on the steel surface for Rubber Wheel test with sand and water from Israel + oil at 20X magnification.**	**Figure 77 Wear track on the steel surface for Rubber Wheel test with sand and water from Israel + oil at 400X magnification.**	**Figure 78 Wear track on the steel surface for Rubber Wheel test with sand and water from Israel + oil at 1500X magnification.**

Casting sand & Israel water	Figure 79 Wear track on the steel surface for Rubber Wheel test with casting sand and water from Israel at 20X magnification.	Figure 80 Wear track on the steel surface for Rubber Wheel test with casting sand and water from Israel at 400X magnification.	Figure 81 Wear track on the steel surface for Rubber Wheel test with casting sand and water from Israel at 1500X magnification.
Casting sand & Faroe Islands water	Figure 82 Wear track on the steel surface for Rubber Wheel test with casting sand and water from the Faroe Islands at 20X magnification.	Figure 83 Wear track on the steel surface for Rubber Wheel test with casting sand and water from Israel at 400X magnification.	Figure 84 Wear track on the steel surface for Rubber Wheel test with casting sand and water from Israel at 1500X magnification.

IPC

The results from the IPC analysis showing the amount of chromium, iron, nickel and copper in the solutions from the rubber wheel test are presented in Table 14 and Figure 85. The concentrations shown in Figure 85 are in a logarithmic scale.

Table 14 Concentration of Cr, Fe, Ni and Cu in the test solutions used in the rubber wheel test.

Condition	Cr [µg/L]	Fe [µg/L]	Ni [µg/L]	Cu [µg/L]
Faroe Island water	0.4219	2.7474	3.5440	5.0075
Faroe Island water + foam	47.6697	1231.1227	71.6108	37.5114
Israel W&S	0.8291	278.1864	7.3804	0.5386
Israel W&S + oil	39.7554	9412.4869	19.1080	15.1005
Israel water & casting sand	0.0749	131.5253	23.2804	3.0182
Faroe Island water & casting sand	0.0000	28.7060	2.9782	3.6525
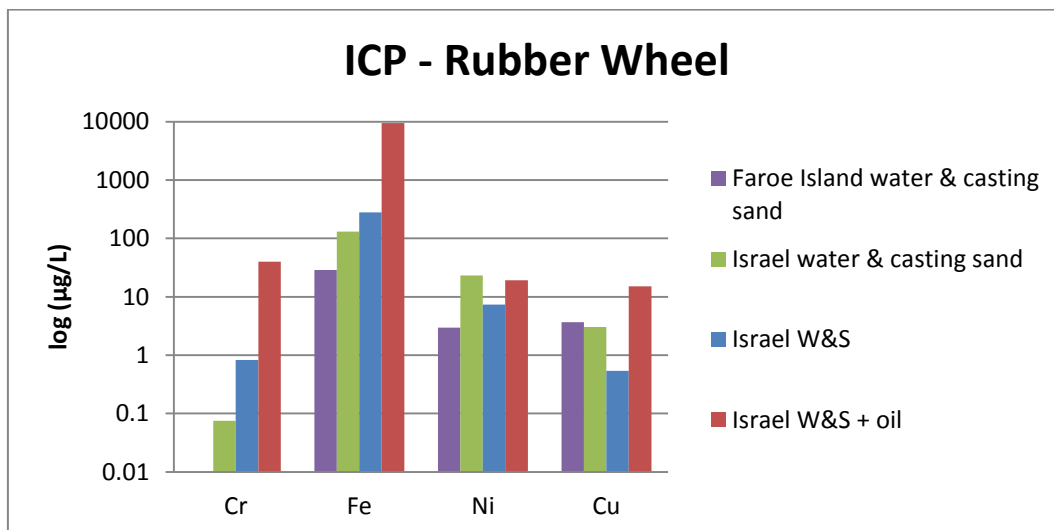
Figure 85 Graphical presentation of the results from the IPC analysis of the Rubber Wheel test on a logartimic scale.

5.5.3 Hyperbaric Soil Abrasion test

The weight loss from the Hyperbaric Soil Abrasion test is presented in Table 15 and Figure 86 shows a graphical presentation of the weight loss. SEM pictures of the worn surfaces are shown in Figure 87 to Figure 92 (Table 16).

Table 15 Weight loss from the Hyperbaric Soil Abrasion test.

Test number	Sample number	Weight loss [g]	Duration [minutes]	Condition
1	1 2	0.0031 0.0037	38	Saturated with water from Israel.
2	1 2	0.0027 0.0034	35	Saturated with water from Israel.
3	1 2	0.0034 0.0038	38	Dry sand.
4	1 2	0.0038 0.0032	38	Dry sand.
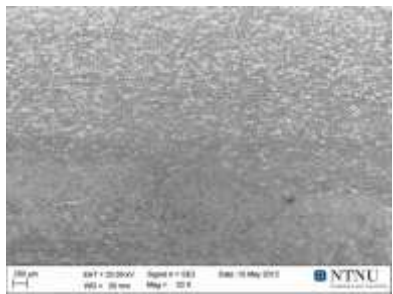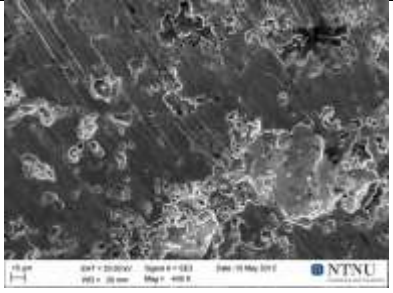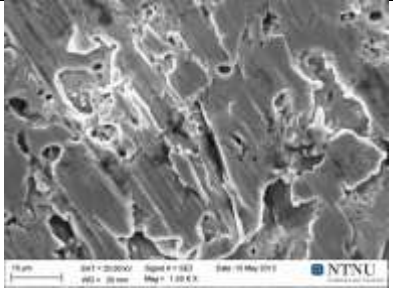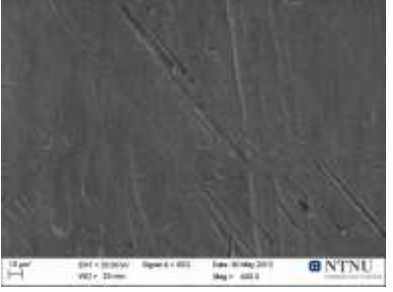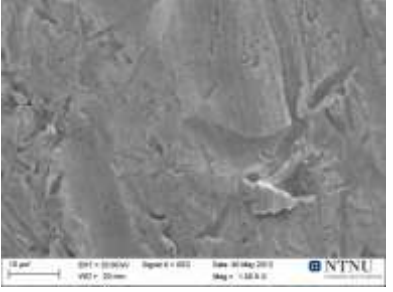
Figure 86 Graphical presentation of the weight loss form the Hyperbaric Soil Abrasion test.

48

Table 16 SEM pictures of the steel surface after Hyperbaric Soil Abrasion test.

Condition	Magnification		
	20X	400X	1500X
Soil saturated with water from Israel	**Figure 87 Wear track on the steel surface after Hyperbaric Soil Abrasion test, saturated with water, at 20X magnification.**	**Figure 88 Wear track on the steel surface after Hyperbaric Soil Abrasion test, saturated with water, at 400X magnification.**	**Figure 89 Wear track on the steel surface after Hyperbaric Soil Abrasion test, saturated with water, at 1500X magnification.**
Dry soil	**Figure 90 Wear track on the steel surface after Hyperbaric Soil Abrasion test, dry, at 20X magnification.**	**Figure 91 Wear track on the steel surface after Hyperbaric Soil Abrasion test, dry, at 400X magnification.**	**Figure 92 Wear track on the steel surface after Hyperbaric Soil Abrasion test, dry, at 1500X magnification.**

6 Discussion

6.1 Titration

The water sample from Israel was obtained from a tunnel being bored underneath the seabed and titration of the water showed that it contained 1.43±0.01 wt. % chloride. Normal sea water contains approximately 3.5 wt. % chloride. However, the water in this case has been filtered through the sand in the seabed, removing some chloride. In addition the bentonite used during soft ground tunnel boring also forces some chloride to be removed. Despite the fact more than half the chloride normally present in sea water is gone, 1.4 wt. % is still enough to cause corrosion.

When it comes to the water sample from the Faroe Islands, they were obtained from a hard rock tunnel. This means that the water had been filtered through rocks over large distances. Because of this filtering, the water contained almost no chloride at all (0.02±0.01 wt. %). However, despite the rock filtering and low chloride content the water had a pH value of 7.7. This means that there have to be some residual contamination in the water.

6.2 Steel characterisation

The microstructure of the steel was found to be martensitic with some small areas with retained austenite. This microstructure is known to have a high hardness, and this was confirmed by a measured hardness of 662±25 VHN. The variations in measured hardness did not give any distinct trend to any of the six areas being harder than the others. The variation may have been caused by microstructural variations, and because the method used was macro indentation, not micro indentation, it was not possible to determine the hardness of each single phase.

The composition of the steel was determined by a hand held XRF-machine, and because of this the result may not as accurate as if it had been conducted on a stationary machine. However, the elements detected are all known to increase the hardenability of the steel. In addition, some of the elements have other effects as well. Such as; increased ductility (Ni), grain refining (V) and retaining hardness at elevated temperatures (Cr and Mo). These are all important to make the steel withstand the environment it is exposed to during boring.

6.3 Rock and soil characterisation

The XRD of the rock from the Faroe Islands showed that the main mineral present was feldspar (79 wt. %), which is only moderately hard, and low quartz content (3 wt. %). This indicates that the rock will not cause much wear on the steel during testing.

The XRD of the sand from Israel on the other hand showed a high quantity of quartz (72 wt. %), which is an abrasive mineral due to its hardness and brittleness. In addition the shape descriptors presented in Figure 45 to Figure 47 shows that the particles geometry are ranging from round and blunt to oblong and sharp edged. The aspect ratios given in Figure 45 give an indication of how oblong the grains are. While the roundness (Figure 46) indicates how the shape of the particle is compared to a circle, where the value 1 indicated that the particle is a circle. However, the two previous shape descriptors do not show how the shape along the perimeter of the particles is. This is covered by the form factor (Figure 47), which give an indication of whether there are blunt or sharp edges around the perimeter. A higher value for the form factor indicates a more rounded

perimeter. These shape descriptors and XRD analysis indicate that the particles in the Israel sand will give significant abrasive wear due to their shape and the quartz content. The quartz particles may also become crushed during testing, which would give additional sharp particles.

6.4 Polarisation curves

The polarisation curves for the water from the Faroe Islands (Figure 48) showed that the corrosion rate at both the anodic and cathodic reactions is reduced quite rapidly. However, when adding foam in to the water a larger potential difference is needed to obtain the same corrosions rate. This may be explained by combining the polarisation curves and the Pourbaix diagram (Figure 93). This shows that the pH of the solutions play significant role. The pH value of the water is 7.7 and the foams pH value is 3.3. As shown in Figure 93, a pH of 3.3 causes the steel to have a much larger possibility to corrode than at pH 7.7. The foam also causes a small drop in the E_{corr} down into the immune area. It is important to remember that the pH values are for the water and the foam only, not a mixture of them. This means that the pH value of the water-foam mixture are somewhat above 3.3.This may also be the reason why the polarisation curves shows that the steel passivate after a while, and do not keep on corroding as the Pourbaix diagram for pH 3.3 indicates.
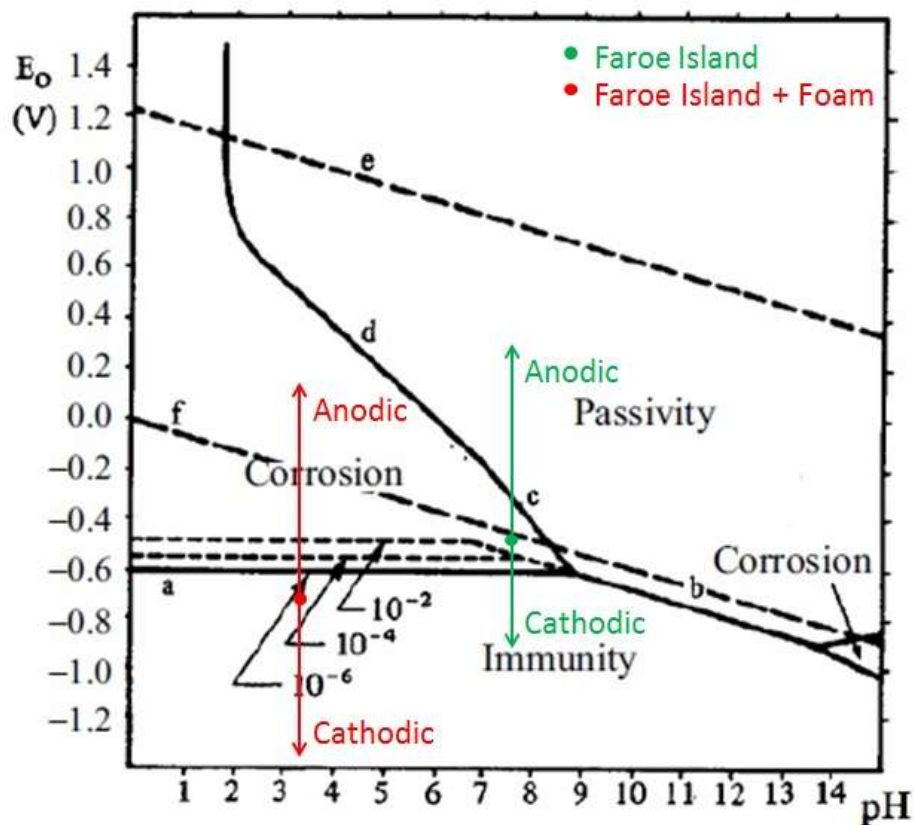
Figure 93 The Pourbaix diagram for iron in water showing the anodic and cathodic potentials from the potentiostat [11].

The polarisation curves for the water from Israel (Figure 49), which contained approximately 1.43 wt. %, showed that there was not much difference between the curves for water only and the water-foam mixture. However, the curves for the water and foam solution shows that the steel tend to passivate quicker. The Pourbaix diagram for 3.5 wt. % NaCl (Figure 94) shows that the

foam has the same effect as for the sample from the Faroe Islands mentioned above. However, the Pourbaix diagram for 3.5 wt. % NaCl shows that the corrosion product $FeCl_2$ will form at the low pH value. This corrosion product may form a protective barrier layer on the surface, explaining the earlier passivation water and foam solution. As for the sample from the Faroe Islands, the pH values are for the water and the foam only, not a mixture of them. Consequently, the real pH value will be above 3.3. However, the formation of $FeCl_2$ will occur even at a pH value of 7, meaning that it still will form during the polarisation. In addition it is important to remember that the Pourbaix diagram shown here are valid for water containing 3.5 wt. % NaCl, while the solution tested has only 1.43 wt. %.

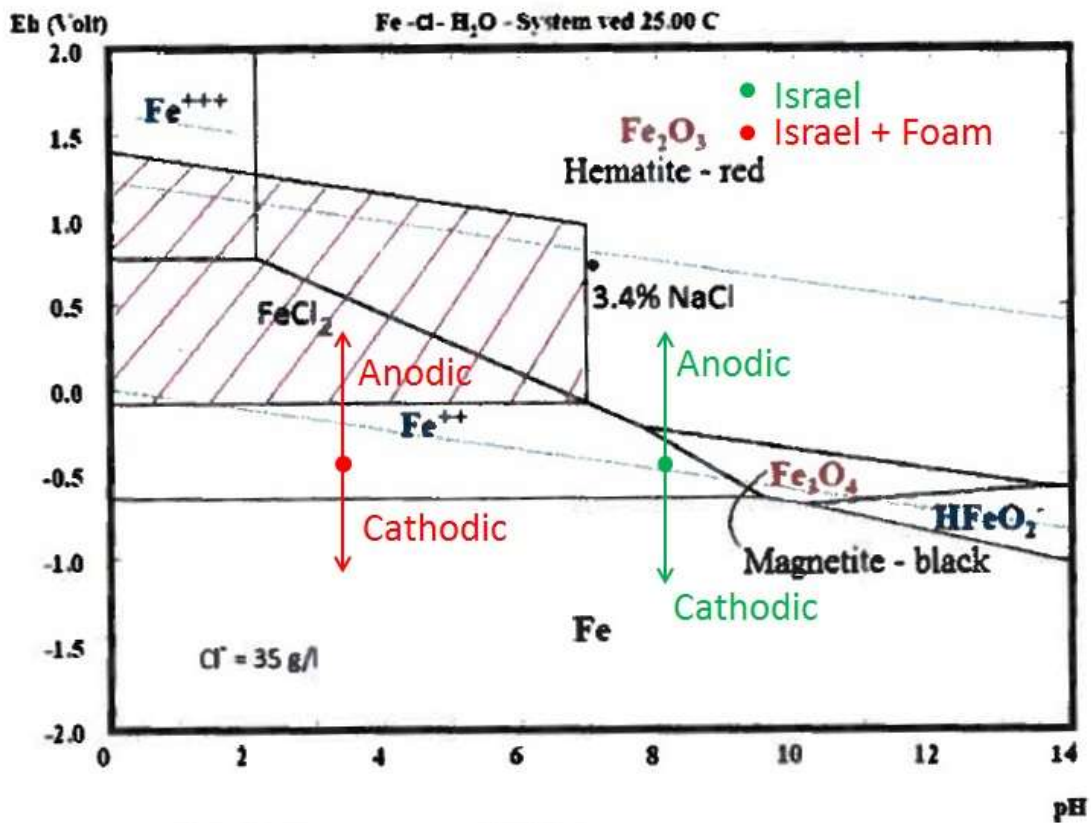**Figure 94 The Pourbaix diagram for iron in 3.5 % NaCl showing the anodic and cathodic potentials from the potentiostat [13].**

6.5 Reciprocating ball-on-plate

The dry rubbing test caused a high COF and a clear wear track on both ball and rocks. The SEM pictures of the rock surface (Figure 59 to Figure 61) clearly show that it has been subjected to forces exceeding yield causing particles to be torn off. It is evident that the particles torn off the rock have caused abrasion stripes on the balls. There is a large quantity of relatively short and narrow abrasion stripes on the surface of the ball (Figure 54). This indicates that the particles torn off the rock surface are small, and have caused abrasion to occur while being removed from the contact area by the sliding motion of the ball. There are also some larger stripes present on the steel surface. These may have been caused by some roughness peaks on the rock surface, such as the one shown in Figure 61. This figure also shows that some of the wear occurring on the rock surface follows the grain boundaries. Despite the evident wear that has occurred on the steel ball, there was no measurable weight loss. This may be due to the high hardness of the steel.

The reciprocal ball-on-plate test performed with water from the Faroe Islands gave a COF that was lower than the one recorded during dry rubbing, but it was still relatively high. Also the size of the wear tracks on both the steel ball and rock surface were reduced, and the number of wear marks became fewer compared to the test with dry rubbing. This may be because although the water was not a good lubricant, it did give some lubrication. Figure 56 shows that in addition to the abrasion stripes on the steel surface, there are a few pits present on the surface. These pits may have been caused by corrosion due to chloride ions in the water. Although the amount of chloride in the water from the Faroe Islands was determined by titration to be 0.02 wt. %, it may have been sufficient to cause the pits. There may also be some additional unknown corrosive elements present in the water, contributing to the formation of these pits. The ICP analysis (Figure 68) shows that all the elements investigated were present in the solution. This shows that some wear has occurred on the steel surface. However, as for the dry rubbing, there was no measurable weight loss on the steel ball after rubbing in water from the Faroe Islands.

The foam-mixture caused a big drop in the COF compared to the two previous tests. The rubbing with foam did not lead to any measurable weight loss either. This may be because the foam caused a lubricating film to occur, presumably EHL, between the two surfaces, preventing contact between them. The SEM pictures of the steel surface (Figure 57 and Figure 58) show that although some abrasion occurred, it was almost no abrasion marks present on the steel surface. Like the COF drop, this also indicates that there has been full film lubrication between the rock and the steel ball, preventing roughness peaks and particles to cause wear. However, the SEM pictures also show that a few pits are present on the steel surface, mainly outside of the contact area between the rock and the ball. The IPC analysis (Figure 68) shows that there was a higher concentration of all the elements measured. This indicates that more wear and corrosion have occurred in the foam-mixture then in water only. However, the SEM pictures show that the amount of abrasive wear on the steel ball was smaller in the foam-mixture. Consequently, the amount of corrosion occurred in the foam-mixture has to be greater than in the water. It is also important to consider the possibility that the foam may contain some of the elements investigated, causing the concentrations to become higher. As for the steel surface, the wear tracks on the rock surface also became smaller when rubbed in the foam-mixture compared to the two previous tests. The wear tracks were so small that they were hard to see by the naked eye,

and also hard to find in the SEM. However, the SEM pictures (Figure 65 to Figure 67) show that some wear have occurred on the rock surface. These pictures also show that most of this wear has occurred along the grain boundaries, probably due to the high pressure from the film formed between the surfaces.

6.6 Rubber Wheel

The combination of casting sand and water from the Faroe Islands gave the least amount of weight loss on the steel sample. Figure 83 and Figure 84 shows that the weight loss was due to abrasion only. It is also evident that the abrasion stripes are most likely caused by particles stuck in on the rubber wheel, causing three-body abrasion to occur. The result from the ICP analysis also shows that this combination had the least amount of wear, giving the lowest concentration of the elements investigated.

The combination of casting sand and water from Israel produced the second lowest weight loss. However, Figure 68 shows that the biggest weight loss was measured after 20 minutes of testing, and afterwards the gradient of the slope for this combination is approximately the same as for casting sand and water from the Faroe Islands. Nevertheless, the gradient for casting sand and water from Israel is somewhat steeper which indicates that more wear have occurred. This is supported by the SEM pictures (Figure 79 to Figure 81), which shows that, in addition to the abrasive wear, some corrosion are present in the form of pits. The ICP results show a bit mixed result, having the highest and third highest concentration of Ni and Cu, respectively. However, for Cr and Fe, which is the steel contains the most of; the concentration is the second lowest, supporting the previous results.

The test with sand and water from Israel (Israel S&W) gave the second highest weight loss of the tests. Figure 70 shows that in addition to the abrasive wear, some corrosion have occurred as well. The occurrence of corrosion is not strange since the water contains 1.43 wt. % chloride ions. From Figure 72 it is possible to see that the corrosion occurs along the abrasive stripes caused by the sand particles. This may be because these grooves act as a crevice, causing crevice corrosion to occur. The IPC analysis shows that the concentration of Cr and Fe are the second highest. This supports the weight loss measurements. However, as for the casting sand and Israel water test, the concentrations of Ni and Cu are the second lowest and the lowest, respectively. This may be because these elements are only present in small quantities (0.04 % Cu and 0.14% Ni) in the steel.

When adding the MEYCO SLF41 foam to the mixture of sand and water from Israel (Israel S&W + Foam), Figure 69 shows that the weight loss was more than halved, and the SEM pictures (Figure 73 to Figure 75) shows that there are little abrasive wear present on the surface. This may be because the foam causes the less sand particles to be present inside the contact area between the rubber wheel and the steel surface. However, the SEM pictures also show that there are more corrosion pits present on the surface with the foam than in the test without foam. These pits may act as initiation points for fatigue and if the cutter disc suffers an impact, such as hammering, they may act as crack initiation points as well.

Adding oil instead of foam caused the highest weight loss of all the tests. The SEM pictures (Figure 76 to Figure 78) show that the amount of abrasive wear on the steel surface increased compared to the test with foam. This shows that in this setting the oil acts as a poor lubricant. In addition to the increased abrasive wear, a significant amount of corrosion pits occurred in this test as well. These pits may have effects equivalent to those in the foam test described above. The IPC results show that the concentration of Cr, Fe and Cu are the highest ones measured, supporting the weight loss measurements. However, as for the previous tests, the Ni content is only the second highest. This may be because of the amount of Ni present in the steel compared to the others, as described previously.

In addition to the comments on the IPC analysis above, it is important to remember that the presents of the elements in the water after testing may have been elevated by corrosion of the steel container holding the solution.

6.7 Hyperbaric Soil Abrasion test

Both of the hyperbaric soil abrasion tests performed, with water saturated sand and dry sand showed a somewhat similar weight loss. However, the SEM pictures in Table 16 show that the wear occurring in the two different conditions. Figure 87 to Figure 89 showed that a great deal of pitting had occurred on the steel surface in the water saturated solution. These corrosion pits may be due to the presents of chloride (1.43 wt. %) in the water. In addition Figure 89 shows that abrasive wear also have occurred. Figure 90 to Figure 92 shows that only abrasive wear had occurred on the steel surface during the dry test. In Figure 91 it is evident that the sand particles mainly have caused ploughing to occur. This can be seen as abrasion stripes with some residual material on each side of the stripe.

The fact that the SEM pictures show that both corrosion and abrasive wear had occurred in the water saturated test and only abrasive wear in the dry test, and still obtaining a similar weight loss, shows that in this test the hardness of the steel and abrasiveness of the sand is more decisive for the weight loss than the corrosivity of the solution.

7 Conclusions

7.1 Reciprocal ball-on-plate
Neither of the tests produced any measurable weight loss.

The dry test produced a high COF and the biggest amount of abrasive wear on both the steel and rock surface. However, there was no measurable weight loss after the tests. This indicates that despite the high OCF during hard rock tunnel boring, the cutter discs do not suffer much wear.

The water from the Faroe Islands reduced the COF and the size of the wear tracks on both the steel and rock surface. However, there was some small corrosion pits occurring on the steel surface. These pits may act as crack initiation point if the disc cutter is exposed to hammering during boring, causing fatigue of even brittle fracture to occur.

The foam solution lowered the COF significantly by producing elastohydrodynamic lubrication (EHL). This resulted in almost no visible wear tracks neither on the steel nor rock surface. However, the foam is causing more pitting to occur on the steel surface, making the disc cutters more vulnerable to fatigue and brittle fracture.

7.2 Rubber Wheel
The combination of sand and water from Israel gave the highest weight loss of the tests without additives. This shows that the conditions present at this tunnel boring site were highly deteriorating.

Adding the MEYCO SLF41 foam caused a reduction in the abrasive wear, and consequently a reduced weight loss. This indicates that the foam sufficient lubrication to prevent contact between the sand particles and the steel surface. However, the foam also caused additional pitting to occur. This increase in corrosivity may be due to the low pH (pH 3.3) of the foam. These pits may cause fatigue to occur or even brittle fracture if the cutter disc encounters some hard geological formations.

Adding the hydraulic oil Shell Tellus S 32 caused the highest weight loss of all. The amount of pitting is equivalent to the foam additive, but the oil did not offer enough lubrication to prevent the sand particles to abrade the steel surface. This shows that adding oil causes more deterioration than without any additive. In addition, the pits may have the same effect as for the foam additive described above.

7.3 Hyperbaric Soil Abrasion test
Both the hyperbaric soil abrasion tests performed, water saturated and dry, showed similar weight loss. This shows that in this test the hardness of the steel and abrasiveness of the sand is more decisive for the weight loss than the corrosivity of the solution.

8 Reference list

1. Girmscheid, G., *Tunnel Boring Machines.* Pract. Period. Struct. Des. Constr., 2003. **8**(3): p. 150.
2. EFNARC, *Specifications and Guidelines for the use of specialist products for Mechanised Tunnelling (TBM) in SOft Ground and Hard Rock.* 2005.
3. Bruland, A., *Hard rock tunnel boring*. 1998, [Tapir]: Trondheim.
4. Norwegian-Tunneling-Society, *Norwegian TBM Tunnelling.* Norwegian Soils and Rock Engineering Association, 1998. **11**: p. 11 - 34.
5. Nilsen, B., et al. *New test methodology for estimating the abrasiveness of soils for TBM tunneling*. in *Rapid Excavation And Tunneling Conference - 2007*. 2007. Toronto, ON, Canada: Society for Mining, Metallurgy and Exploration.
6. Jakobsen, P.D., F. Dahl, and L. Langmaack, *Reduction of hard Rock Abrasiveness using Foam Agents.* Tunnel, 2009. **8**.
7. Stachowiak, G.W. and A.W. Batchelor, *Engineering Tribology*. Engineering Tribology (Third Edition). 2006, Burlington: Butterworth-Heinemann.
8. Williams, J.A., *Engineering Tribology*. 1994: Oxford University Press Inc.
9. Czichos, H., *TRIBOLOGY - a systems approach to the science and technology of friction, lubrication and wear.* 1978, Elsevier Scientific Publishing Company.
10. Russ, J.C., *The Image Processing Handbook*. Fifth Edition ed. 2006: CRC Press.
11. Bardal, E., *Korrosjon og Korrosjonsvern*. 2001: Tapir Akademiske Forlag.
12. Rieve, R.W. and H.H. Uhling, *Corrosion and Corrosion Control*. 4th ed. 2008: WILEY.
13. *HSC Chemistry 6.1 software*, Chemistry software LTD, UK.
14. Mischler, S., *Triboelectrochemical techniques and interpretation methods in tribocorrosion: A comparative evaluation.* Tribology International, 2008. **41**(7): p. 573-583.
15. Dieter, L., *Tribocorrosion*, in *Corrosion and Surface Chemistry of Metals*. 2007, EFPL Press. p. 415-460.
16. Zum Gahr, K.-H., *Microstructure and wear of materials*. Vol. 10. 1987, Amsterdam: Elsevier. ix, 560 p.
17. Rasband, W., *http://rsbweb.nih.gov/ij/*. 2002-2005.
18. MEYCO-BASF. *ABR 5*. 2011; Available from: http://www.meyco.basf.com/en/meyco_solutions/TDS/TBM/antiwearanddustagents/ABR%205/Pages/default.aspx.
19. MEYCO-BASF. *SLF41*. 2012; Available from: http://www.meyco.basf.com/en/meyco_solutions/TDS/TBM/soilconditioningfoams/slf41/Documents/TDS_MEYCO_SLF_41.pdf.
20. Shell. *Tellus Oil S 32*. 2012; Available from: http://www.epc.shell.com/Docs/GSAP_msds_00083924.PDF.

9 Appendices

9.1 Appendix A

9.1.1 Weight loss from rubber wheel
Table 17 Weight loss from rubber wheel tests.

Condition	Test number	Weight loss [g]						
		0	10	20	30	40	50	60
		[minutes]						
Israel sand & water	1	0.0000	0.0018	0.0197	0.0266	0.0369	0.0489	0.0631
Israel sand & water	2	0.0000	0.0034	0.0132	0.0253	0.0330	0.0423	0.0522
Israel sand & water + Foam	1	0.0000	0.0044	0.0080	0.0122	0.0155	0.0194	0.0236
Israel sand & water + Foam	2	0.0000	0.0039	0.0079	0.0115	0.0153	0.0194	0.0232
Israel sand & water + Oil	1	0.0000	0.0080	0.0227	0.0405	0.0589	0.0717	0.0892
Israel sand & water + Oil	2	0.0000	0.0144	0.0287	0.0446	0.0595	0.0760	0.0925
Casting sand & Israel water	1	0.0000	0.0008	0.0017	0.0024	0.0033	0.0044	0.0056
Casting sand & Israel water	2	0.0000	0.0012	0.0086	0.0093	0.0103	0.0113	0.0123
Casting sand & Faroe Islands water	1	0.0000	0.0018	0.0025	0.0029	0.0035	0.0043	0.0046
Casting sand & Faroe Islands water	2	0.0000	0.0010	0.0018	0.0020	0.0024	0.0027	0.0031